research paper

STRUCTURAL CHEMISTRY

ISSN 2053-2296

Pharmaceutical salts of emoxypine with dicarboxylic acids

Alex N. Manin,[a] Alexander P. Voronin,[a] Ksenia V. Drozd,[a] Andrei V. Churakov[b] and German L. Perlovich[a]*

[a]G. A. Krestov Institute of Solution Chemistry of the Russian Academy of Sciences, 1 Akademicheskaya St., Ivanovo 153045, Russian Federation, and [b]Institute of General and Inorganic Chemistry of the Russian Academy of Sciences, 31 Leninsky Prosp., Moscow 119991, Russian Federation. *Correspondence e-mail: glp@isc-ras.ru

Received 18 April 2018
Accepted 16 May 2018

Edited by D. S. Yufit, University of Durham, England

Keywords: emoxypine; antioxidant drug; multicomponent crystals; crystal structure; lattice energy; computational chemistry; melting point; solubility.

CCDC references: 1836239; 1836241; 1836240

Supporting information: this article has supporting information at journals.iucr.org/c

New salt forms of the antioxidant drug emoxypine (EMX, 2-ethyl-6-methylpyridin-3-ol) with pharmaceutically acceptable maleic (Mlt), malonic (Mln) and adipic (Adp) acids were obtained {emoxypinium maleate, $C_8H_{12}NO^+\cdot C_4H_3O_4^-$, [EMX+Mlt], emoxypinium malonate, $C_8H_{12}NO^+\cdot C_3H_3O_4^-$, [EMX+Mln], and emoxypinium adipate, $C_8H_{12}NO^+\cdot C_6H_9O_4^-$, [EMX+Adp]} and their crystal structures determined. The molecular packing in the three EMX salts was studied by means of solid-state density functional theory (DFT), followed by QTAIMC (quantum theory of atoms in molecules and crystals) analysis. It was found that the major contribution to the packing energy comes from pyridine–carboxylate and hydroxy–carboxylate heterosynthons forming infinite one-dimensional ribbons, with [EMX+Adp] additionally stabilized by hydrogen-bonded $C(9)$ chains of Adp^- ions. The melting processes of the [EMX+Mlt] (1:1), [EMX+Mln] (1:1) and [EMX+Adp] (1:1) salts were studied and the fusion enthalpy was found to increase with the increase of the calculated lattice energy. The dissolution process of the EMX salts in buffer (pH 7.4) was also studied. It was found that the formation of binary crystals of EMX with dicarboxylic acids increases the EMX solubility by more than 30 times compared to its pure form.

1. Introduction

2-Ethyl-6-methylpyridin-3-ol (emoxypine, EMX) is a Russian-made drug that belongs to the class of 3-hydroxypyridines, which are structural analogues of vitamin B6. Emoxypine produces an antihypoxic, nootropic, anticonvulsant and anxiolytic action, and increases the body's ability to cope with stress (Borovikov, 2016). Since emoxypine in its pure form has a rather low solubility, it is used in the pharmaceutical industry as the hydrochloride (Emoxipine) or succinate salts (Mexidol or Mexifin). Both agents have antioxidant properties due to their ability to interact with Fe^{2+} ions and water-soluble radicals (*e.g.* the superoxide anion) and to improve the efficiency of the endogenous antioxidant system (Chesnokova *et al.*, 2015). Mexidol is currently more popular as it is less toxic than Emoxipine (Levitskaya *et al.*, 2016). A recently discovered salt of emoxypine with *N*-acetylglutamic acid was shown to improve biological action in rats (Yasnetsov *et al.*, 2010, 2012). The crystal structures of known EMX salts show that emoxypine is able to form polymorphic salt forms (Chernyshev *et al.*, 2013), as well as salts with different API/counter-ion ratios (API is an active pharmaceutical ingredient) (Lyakhov *et al.*, 2012*b*).

This strategy of solubility and bioavailability enhancement by obtaining new API salts with different organic counter-ions is more and more often becoming an alternative to obtaining salts with chloride ions (Paulekuhn *et al.*, 2007). For example,

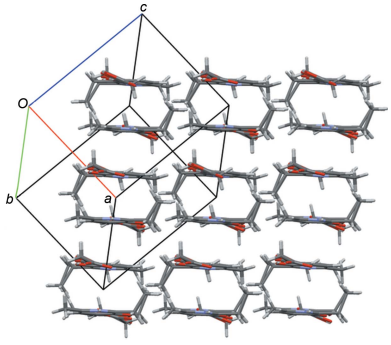

salts of APIs with dicarboxylic acids improve the solubility of the drug compounds by a factor of dozens (Surov *et al.*, 2015; Basavoju *et al.*, 2006; Bruni *et al.*, 2013). In some cases, dicarboxylic acid salts have higher solubility values than the hydrochloride salts (Manin *et al.*, 2015). Besides, most dicarboxylic acids are considered pharmaceutically acceptable {Orange book, 2018 [*Orange Book: Approved Drug Products with Therapeutic Equivalence Evaluations* (March 2018), http://www.accessdata.fda.gov/scripts/cder/ob/, US Food and Drug Administration]; Pudipeddi *et al.*, 2002} and potentially less harmful for the gastrointestinal tract compared to HCl due to the lower pK_a of the acid (Bansal *et al.*, 2008).

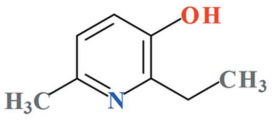

Emoxypine, **EMX**

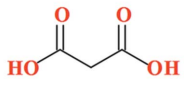

Malonic acid, **Mln**

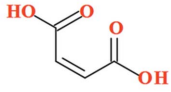

Maleic acid, **Mlt**

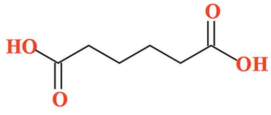

Adipic acid, **Adp**

Scheme 1

Thus, it was shown that the change of counter-ion significantly affects the *in vivo* performance of commercially available salt forms of EMX and this method was chosen in the search of new crystal forms with enhanced properties. First, a combined experimental and theoretical study should be conducted in order to assess the influence of the molecular and crystal structures on pharmaceutically relevant properties. There are approaches linking the solubility of pharmaceutical crystals with its melting point (Perlovich, 2014; Abramov, 2015) and theoretical lattice energy evaluated by solid-state density functional theory (DFT) (Voronin *et al.*, 2016). The literature survey of multicomponent crystals of dicarboxylic acids with various APIs conducted in our earlier work (Manin *et al.*, 2015) has shown the influence of the melting point and carbon chain length of the salt/cocrystal former on the potential solubility of the API. However, variations of the experimental conditions and solubility data do not allow the predictive use of named correlations for individual APIs without known reference solubility and melting point/lattice energy values, which require a preliminary screening study.

In the present work, emoxypine was reacted with a series of dicarboxylic acids, *i.e.* malonic (Mln), maleic (Mlt) and adipic (Adp) acids (Scheme 1), giving emoxypinium maleate, [EMX+Adp], emoxypinium malonate, [EMX+Mln], and emoxypinium adipate, [EMX+Adp]. All the salt coformers produced new crystal forms. This article focuses on the theoretical and experimental study of emoxypine salt design, and on the physicochemical properties of the malonate, maleate and adipate salts compared to the emoxypine free base.

2. Experimental

2.1. Compounds and solvents

Emoxypine was obtained from emoxypine hydrochloride (see §S1 in the supporting information). Malonic acid (99%), maleic acid (99%) and adipic acid (99%) were purchased from Acros Organics. All reagents were available commercially and were used as received without further purification.

2.2. Crystallization procedure

Emoxypine and dicarboxylic acid in a 1:1 molar ratio were dissolved in a methanol–acetone mixture (1:1 *v*:*v*) and stirred until a clear solution was obtained. The solution was kept in a fume hood at room temperature. Diffraction-quality crystals of the emoxypine salts were grown over a period of 3–4 d. The crystals obtained from the crystallization batches were dried in air before being subjected to further analysis.

2.3. Refinement

Crystal, data collection, and structure refinement details are summarized in Table 1. All H atoms were found in difference Fourier syntheses and refined isotropically. The powder X-ray diffraction data were recorded under ambient conditions in Bragg–Brentano geometry with a Bruker D8 Advance diffractometer with Cu $K\alpha_1$ radiation (λ = 1.5406 Å). Single-crystal X-ray diffraction studies were performed at the Centre of Shared Equipment of IGIC RAS.

2.4. Differential scanning calorimetry (DSC)

The thermal analysis was carried out using a PerkinElmer DSC 4000 differential scanning calorimeter with a refrigerated cooling system (USA). The sample was heated in sealed aluminum sample holders at the rate of 10°C min^{-1} under a nitrogen atmosphere. The unit was calibrated with indium and zinc standards. The accuracy of the weighing procedure was ±0.01 mg.

2.5. Thermogravimetric analysis (TGA)

TGA was performed on a TG 209 F1 Iris thermomicrobalance (Netzsch, Germany). Approximately 10 mg of the sample was added to a platinum crucible. The samples were heated at a constant heating rate of 10°C min^{-1}. The samples were purged with a stream of flowing dry Ar throughout the experiment at 30 ml min^{-1}.

2.6. Aqueous dissolution experiments

The dissolution measurements were carried out by the shake-flask method in a phosphate buffer with pH 7.4 at 25±0.1°C. An excess amount of each sample was suspended in the respective buffer solution in Pyrex glass tubes. The amount of the drug dissolved was measured by taking aliquots of the respective media. The solid phase was removed by isothermal

Table 1
Experimental details.

	[EMX+Mlt]	[EMX+Mln]	[EMX+Adp]
Crystal data			
Chemical formula	$C_8H_{12}NO^+\cdot C_4H_3O_4^-$	$C_8H_{12}NO^+\cdot C_3H_3O_4^-$	$C_8H_{12}NO^+\cdot C_6H_9O_4^-$
M_r	253.25	241.24	283.32
Crystal system, space group	Orthorhombic, *Pccn*	Triclinic, $P\overline{1}$	Triclinic, $P\overline{1}$
Temperature (K)	150	150	150
a, b, c (Å)	26.571 (3), 6.9074 (8), 13.5152 (16)	8.9211 (7), 10.5301 (8), 13.7175 (10)	8.7831 (17), 8.9442 (17), 9.6114 (18)
α, β, γ (°)	90, 90, 90	80.0535 (11), 86.3313 (11), 66.5117 (10)	77.301 (3), 76.142 (3), 85.677 (3)
V (Å^3)	2480.6 (5)	1164.07 (15)	714.9 (2)
Z	8	4	2
Radiation type	Mo $K\alpha$	Mo $K\alpha$	Mo $K\alpha$
μ (mm^{-1})	0.11	0.11	0.10
Crystal size (mm)	0.35 × 0.20 × 0.20	0.40 × 0.20 × 0.05	0.45 × 0.40 × 0.30
Data collection			
Diffractometer	Bruker SMART APEXII	Bruker SMART APEXII	Bruker SMART APEXII
Absorption correction	Multi-scan (*SADABS*; Bruker, 2008)	Multi-scan (*SADABS*; Bruker, 2008)	Multi-scan (*SADABS*; Bruker, 2008)
T_{min}, T_{max}	0.964, 0.979	0.958, 0.995	0.957, 0.971
No. of measured, independent and observed [$I > 2\sigma(I)$] reflections	19445, 2713, 2282	12144, 5599, 4307	6841, 3122, 2569
R_{int}	0.026	0.020	0.021
$(\sin\theta/\lambda)_{max}$ (Å^{-1})	0.639	0.661	0.639
Refinement			
$R[F^2 > 2\sigma(F^2)]$, $wR(F^2)$, S	0.037, 0.101, 1.04	0.039, 0.108, 1.03	0.041, 0.114, 1.05
No. of reflections	2713	5599	3122
No. of parameters	223	427	265
H-atom treatment	All H-atom parameters refined	All H-atom parameters refined	All H-atom parameters refined
$\Delta\rho_{max}$, $\Delta\rho_{min}$ (e Å^{-3})	0.23, −0.19	0.33, −0.23	0.26, −0.23

Computer programs: *APEX2* (Bruker, 2008), *SAINT* (Bruker, 2008) and *SHELXTL* (Sheldrick, 2008).

filtration (Rotilabo® syringe filter, PTFE, 0.2 µm), and the concentration was determined by suitable dilution with a Cary 50 UV–Vis spectrophotometer (Varian, Australia) at the reference wavelength. The results are stated as the average of at least three replicated experiments. The concentrations were calculated according to the established calibration curve.

2.7. Computational procedure

The solid-state DFT computations were performed with the *CRYSTAL14* package (Dovesi *et al.*, 2014) at the B3LYP/6-31G(d,p) level of theory. The D2 dispersion correction proposed by Grimme (2006) was used both in structure optimization and in wavefunction calculation for AIM (atoms in molecules) analysis. Based on the vibrational frequency analysis (Pascale *et al.*, 2004), all the optimized structures were found to correspond to the minimum point on the potential energy surface.

The quantum topology analysis was performed in the *Topond14* (Gatti *et al.*, 1994) software currently built into the *CRYSTAL14* suite. The (3;−1) critical points were found using a standard algorithm and the following quantities were computed in the bond-critical point: electron density, ρ_b, its Laplacian, $\nabla^2\rho_b$, and the positively defined local electronic kinetic energy G_b.

The energy of a particular noncovalent interaction, E_{int}, was computed using the following equation (Mata *et al.*, 2011):

$$E_{int}\ [\text{kJ mol}^{-1}] = 1124 G_b\ [\text{atomic units}]. \quad (1)$$

The lattice energy, E_{latt}, was estimated as the sum of the energies of the unique intermolecular interactions in an asymmetric unit (Dominiak *et al.*, 2012):

$$E_{latt} = \sum_i \sum_{j<i} E_{int,j,i}. \quad (2)$$

The calculation scheme was proved to successfully predict the energies of noncovalent interactions of various types and the sublimation enthalpies of single and multicomponent crystals (Vener *et al.*, 2014, and references therein).

3. Results and discussion

According to the pK_a rule, ionized acid–base complexes are observed exclusively for $\Delta pK_a > 4$ and non-ionized acid–base complexes are observed exclusively for $\Delta K_a < -1$ (Cruz-Cabeza, 2012). In the ΔK_a interval between 0 and 3, the probabilities of the formation of salts and cocrystals are practically equal. The difference between the K_a of emoxypine (p$K_{a,1}$ = 6.49 and p$K_{a,2}$ = 10.05; Chemicalize, 2018) and the first ionization constants of malonic acid (p$K_{a,1}$ = 2.83 and p$K_{a,2}$ = 5.69), maleic acid (p$K_{a,1}$ = 1.90 and p$K_{a,2}$ = 6.07) and adipic acid (p$K_{a,1}$ = 4.43 and p$K_{a,2}$ = 5.41) are negative, which indicates that salt formation is expected.

Table 2
Geometric parameters (Å, °), graph-set notations and QTAIMC energies (E_{HB})* of hydrogen bonds in the studied salt forms of EMX.

Interaction	D—H	H···A	D···A	D—H···A	E_{HB} (kJ mol^{-1})	Graph-set notation
[EMX+Mlt] (1:1)						
O11—H11···O14*	1.13 (2)	1.30 (2)	2.4288 (14)	176 (2)	88.2	E(7)
O1—H12···O^{-}13^{i}	0.87 (2)	1.71 (2)	2.5804 (13)	178.5 (19)	54.1	D
N^{+}1—H1···O12	0.936 (16)	1.795 (17)	2.7165 (14)	167.5 (14)	36.8	D
[EMX+Mln] (1:1)						
O31—H31···O34*	1.09 (2)	1.38 (2)	2.4410 (13)	162 (2)	68.9	E(6)
O41—H41···O44*	1.04 (2)	1.44 (2)	2.4428 (12)	162 (2)	65.1	E(6)
O1—H12···O^{-}33	0.901 (19)	1.69 (2)	2.5925 (13)	175.0 (17)	53.6	D
O2—H22···O^{-}43	0.96 (2)	1.62 (2)	2.5610 (12)	167.6 (19)	51.5	D
N^{+}2—H21···O32	0.927 (17)	1.800 (17)	2.7196 (13)	170.9 (15)	34.8	D
N^{+}1—H11···O42^{ii}	0.918 (15)	1.850 (16)	2.7604 (13)	171.1 (13)	30.9	D
[EMX+Adp] (1:1)						
O11—H11···O^{-}13^{iii}	1.07 (3)	1.40 (3)	2.4639 (15)	176 (2)	72.5	C(9)
O1—H2···O14^{iv}	0.90 (2)	1.66 (2)	2.5355 (12)	163 (2)	59.9	D
N^{+}1—H1···O12	0.90 (2)	1.83 (2)	2.7181 (14)	167.6 (16)	36.3	D

Note: (*) intramolecular hydrogen bond. Symmetry codes: (i) $x-\frac{1}{2}, -y+1, -z+\frac{1}{2}$; (ii) $x-1, y+2, z+1$; (iii) $x-1, y, z$; (iv) $x-1, y+1, z-1$.

The literature data show that emoxypine is able to form polymorphic salts (Chernyshev *et al.*, 2013), as well as salts with different stoichiometric ratios (Lyakhov *et al.*, 2012*b*) and different ionization states with dicarboxylic acids (Lyakhov *et al.*, 2012*a*). Therefore, special attention was paid to varying the experimental conditions in an attempt to discover possible multiple crystal forms for one binary system.

The screening was conducted using the method of slow crystallization from solution. The solvents were methanol, ethanol, acetonitrile, acetone, tetrahydrofuran, ethyl acetate and mixtures of these solvents. The screening experiments yielded three novel crystal forms of EMX with maleic, malonic and adipic acids (see Table S1 in the supporting information).

3.1. Crystal structures of the salts

An emoxypine molecule contains two sites available for hydrogen bonding, namely a hydroxy group and a pyridine ring. The core of the molecule is essentially planar; however, substitution of the *ortho* positions of the N atom with alkyl groups prevents the formation of planar synthons, such as a common $R_2^2(9)$ acid–pyridine heterosynthon. Since the alkyl H atoms are located out of the main plane of the EMX molecule, the coordinated carboxyl groups are not parallel to the EMX plane, which leads to twisted acid–pyridine synthons. Since the number of hydrogen-bond-acceptor sites in the EMX–dicarboxylic acid system exceeds the number of hydrogen-bond donors (five against three), C—H···O contacts are also likely to be observed to saturate the remaining acceptors according to Etter's rules (Etter, 1990).

The crystallographic data for the emoxypine salts are summarized in Table 1, and the asymmetric units of the EMX salts with displacement ellipsoids, along with the packing arrangements of the salts, are shown in Figs. 1–3. The single-crystal X-ray diffraction data confirm the protonation of the pyridine ring of EMX by acid groups of the salt formers, as evidenced by the proton location and bond-length distribution (Table 2).

The [EMX+Mlt] salt crystallizes in the orthorhombic *Pccn* space group. The asymmetric unit of [EMX+Mlt] includes one emoxypine cation and one maleate anion with a strong intra-ion hydrogen bond (Fig. 1*a*). The EMX and Mlt ions are held together by hydrogen bonds of two types, *i.e.* a charge-assisted N^{+}—H···O and a neutral O—H···O hydrogen bond, leading

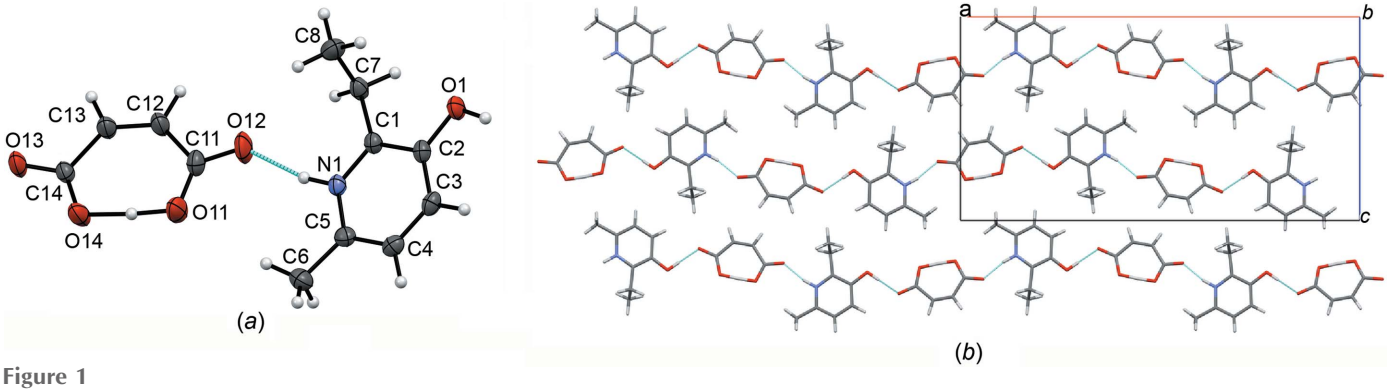

Figure 1
(*a*) The hydrogen-bonded supramolecular asymmetric unit in the crystal structure of [EMX+Mlt] (displacement ellipsoids are drawn at the 50% probability level) and (*b*) a molecular packing projection for [EMX+Mlt].

to the formation of infinite chains along the *a* axis. The chains, in their turn, are held together by weaker intermolecular interactions (Fig. 1*b*).

The [EMX+Mln] salt crystallizes in the triclinic $P\overline{1}$ space group. The asymmetric unit of [EMX+Mln] includes two emoxypine cations and two hydrogen malonate anions (Fig. 2*a*). Similar to the [EMX+Mlt] crystal, the anion adopts a cyclic conformation with an intra-ion hydrogen bond. The EMX and Mln ions form an infinite chain, in which each of the two symmetrically independent ions is held together by one $N^+—H\cdots O$ and one $O—H\cdots O$ hydrogen bond (Fig. 2*b*). It is interesting to note that alternation of the orientation of the anions is observed in chains of the emoxypine malonate and maleate salts, while the orientation of the EMX ions changes only in [EMX+Mlt]. Neighbouring chains of the hydrogen-bonded molecules lie above each other and form tunnel-like structures. The chains are equidistant from each other and are held together by π–π interactions (Fig. 2*c*).

The [EMX+Adp] salt crystallizes into the triclinic $P\overline{1}$ space group. The asymmetric unit of [EMX+Adp] contains one emoxypine cation and one adipate anion (Fig. 3*a*). The EMX molecules are linked with neighbouring molecules of adipic acid by $O—H\cdots O^-$ and $N^+—H\cdots O$ charge-assisted hydrogen bonds and form infinite chains. These chains are linked with each other *via* the adipic acid molecules by $O—H\cdots O$ hydrogen bonds (Fig. 3*b*). The planes formed in this way lie at a distance of 3.18 Å from each other (Fig. 3*c*).

3.2. Pattern of intermolecular interactions

In order to achieve a better understanding of the driving forces responsible for emoxypine salt formation, the molecular packing in the three EMX salts was studied by means of solid-state DFT, followed by QTAIMC analysis. The Bader analysis of periodic electron density allowed us to arrange the main hydrogen-bonding motifs by energy.

Table 3
Contributions of different types of stabilizing noncovalent interactions into the lattice energy* of studied EMX salts.

Crystal	[EMX+Mlt]	[EMX+Mln]	[EMX+Adp]
E_{latt}	226.3	213.7	315.8
ΣE(Hydrogen bonds)	90.8 (40.1%)	85.4 (39.9%)	168.8 (53.4%)
ΣE(C—H···O)	70.1 (31.0%)	80.1 (37.5%)	88.6 (28.1%)
ΣE(C—H···π)	9.0 (4.0%)	10.2 (4.8%)	16.3 (5.2%)
ΣE(H···H)	29.7 (13.1%)	15.4 (7.2%)	26.3 (8.3%)
ΣE(π–π)	26.6 (11.8%)	22.7 (10.6%)	15.9 (5.0%)
E(EMX–EMX)	49.0 (21.7%)	41.8 (19.5%)	25.6 (8.1%)
E(EMX–acid)	167.7 (74.1%)	153.0 (71.6%)	192.1 (60.8%)
E(acid–acid)	9.5 (4.2%)	18.9 (8.9%)	98.1 (31.1%)

Note: (*) all the energies are given in kJ mol^{-1} and as a % of the E_{latt} value

In the [EMX+Mlt] crystal, the extra strong short ($O\cdots O$ = 2.43 Å) intramolecular $O11—H11\cdots O14^-$ hydrogen bond (Steiner, 2002) in the Mlt^- anion was found to be the strongest noncovalent interaction (Table 2, and Table S2 of the supporting information). An unusually short $O\cdots O$ distance and a high ρ_b value at the (3;−1) point indicated the partially covalent nature of this interaction (Gatti, 2005).

Due to the cyclic conformation, the Mlt and Mln ions do not form any strong bonds with each other, and acid–acid interactions make up less than 10% of the lattice energy (Table 3). Thus, the structure is mainly stabilized by EMX–acid and EMX–EMX interactions.

If the conformational change leading to reduction of symmetry in [EMX+Mln] is not taken into account, both

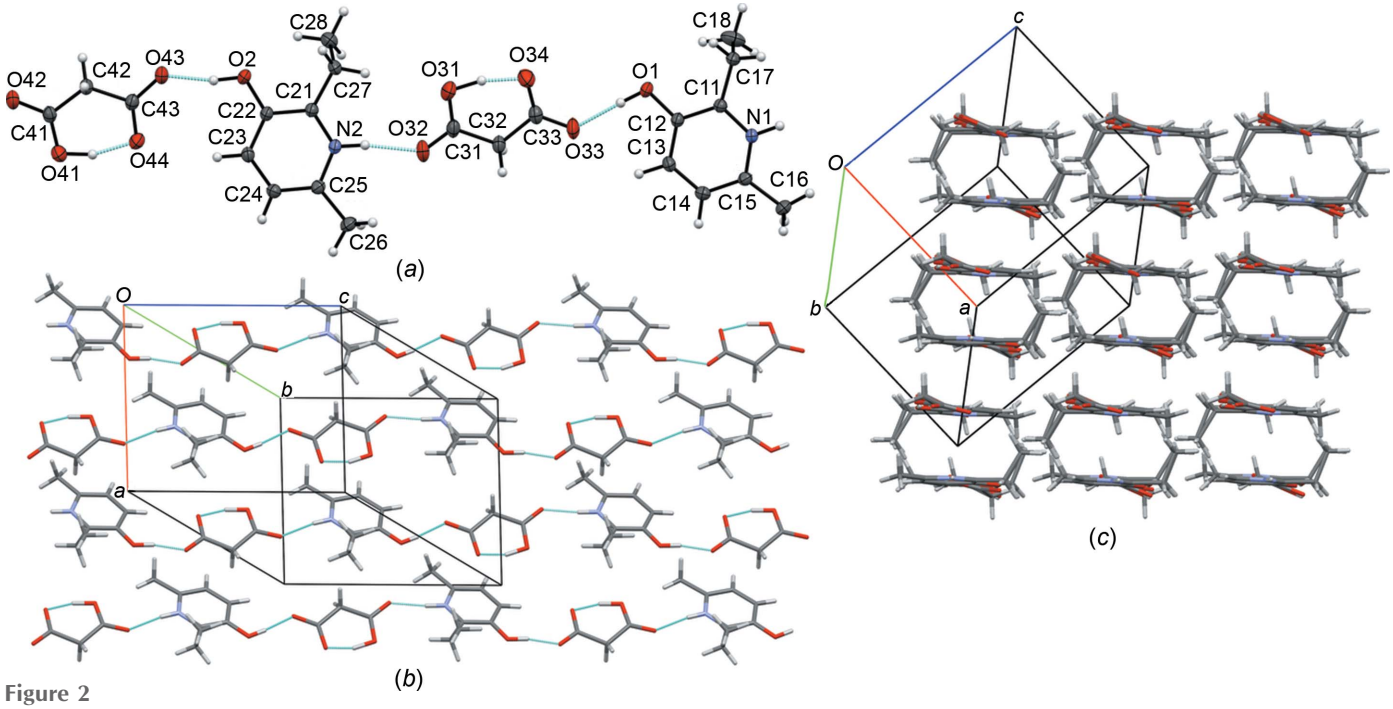

Figure 2
(*a*) The hydrogen-bonded asymmetric unit in the crystal structure of [EMX+Mln], consisting of four ions (the displacement ellipsoids are drawn at the 50% probability level), and (*b*)/(*c*) molecular packing projections for [EMX+Mln].

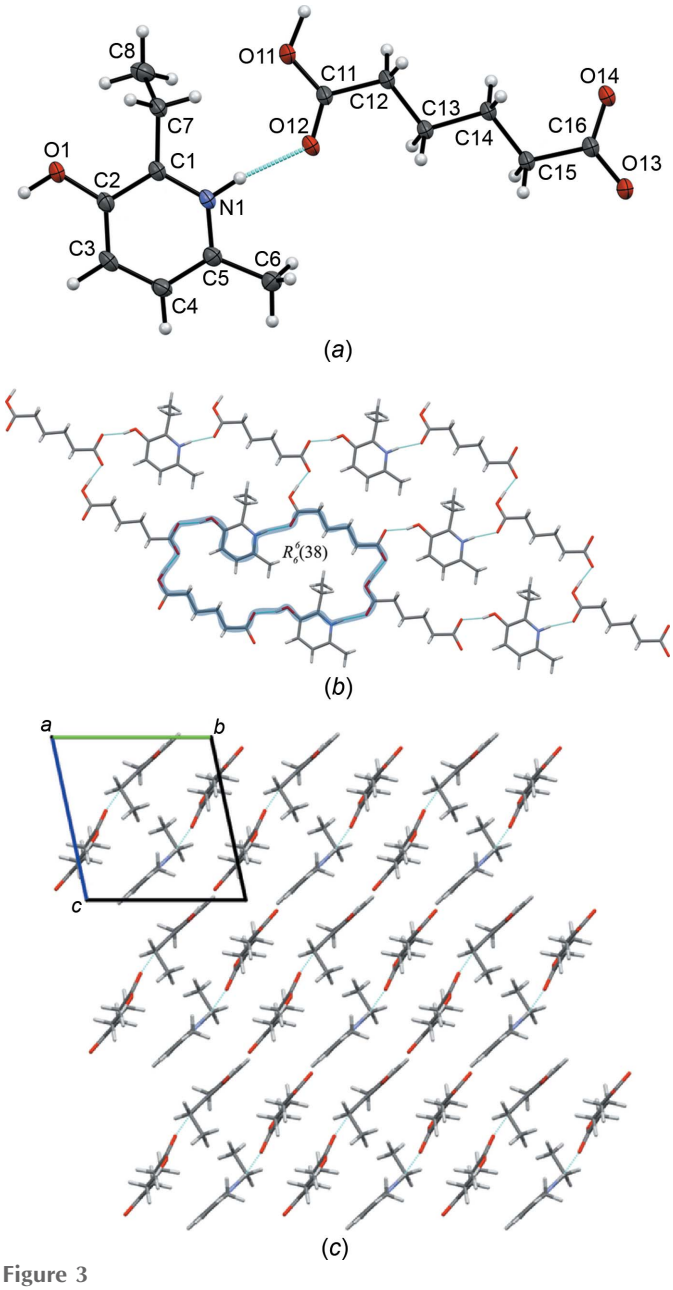

Figure 3
(*a*) The asymmetric unit in the [EMX+Adp] crystal (displacement ellipsoids are drawn at the 50% probability level), consisting of two EMX molecules and an adipate ion. (*b*) The $R_6^6(38)$ hydrogen-bonded ring motif formed by two EMX molecules and four adipate ions in the crystal, held together by charge-assisted N$^+$—H···O and O—H···O$^-$ hydrogen bonds. (*c*) A molecular packing projection for [EMX+Adp].

crystals show packing similarities reflected by QTAIMC results. The pattern of noncovalent interactions in the maleate and malonate salts is hydrogen-bonded EMX–acid chains held together by weaker interactions. The O atoms are coordinated within heterosynthons in [EMX+Mlt] in a fashion similar to [EMX+Adp], with three additional C—H···O contacts for the acid–pyridine hydrogen bond and a stronger single C—H···O contact for the hydroxy–acid bond (Fig. 4). The total energy gains within these synthons are similar: 65 kJ mol^{-1} for hydroxy–carboxylate and 58 kJ mol^{-1} for pyridine–carboxylate.

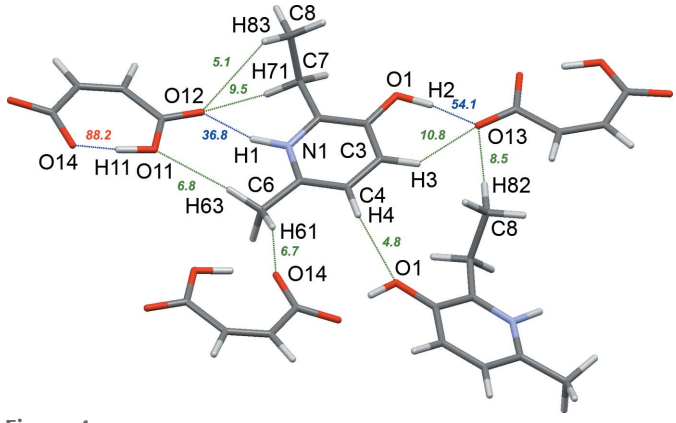

Figure 4
Part of the crystal lattice with noncovalent interactions in the [EMX+Mlt] salt. Hydrogen bonds are shown as blue lines and the main C—H···O contacts are shown as green lines. The numbers represent the energies of particular noncovalent interactions in kJ mol^{-1}, with red numbers corresponding to intramolecular contacts.

Taken together, these interactions within the chain contribute more than 50% to the crystal lattice energy.

The ethyl-group orientation within the chain alternates due to the twofold roto-translational symmetry. Due to the wavelike shape of the parallel layers shown in Fig. 1(*b*) and a relatively small (about 3.5 Å) interlayer distance, π-stacking interactions are likely to be observed in the studied system. The total energy of the interactions within the stack is 32 kJ mol^{-1}, or 14% of $E_{\rm latt}$, of which 18 kJ mol^{-1} comes from C7/C8—H···O contacts between the nearest chains and 27 kJ mol^{-1} from the π-stacking interactions between the non-H atoms. An additional 22 kJ mol^{-1} comes from the H···H and C—H···C contacts of alkyl fragments with the surrounding atoms.

A number of C—H···O and H···H contacts between the EMX and Mlt molecules combine the adjacent stacks of chains into corrugated sheets, which leads to a 36 kJ mol^{-1} gain in the stabilization energy. The relatively strong C8—H82···O13 (8.5 kJ mol^{-1}) and C6—H61···O14 contact (6.7 kJ mol^{-1}), and the supporting H···H interactions distort the parallel orientation of adjacent hydroxy–acid dimers. The total lattice energy of [EMX+Mlt] evaluated using equation 2 is 226.3 kJ mol^{-1}.

The asymmetric unit in [EMX+Mln] contains two EMX molecules with a nearly identical conformation, differing only in torsion angle τ (see Fig. 5) and two molecules of Mln are rotated at about 180° relative to each other. While all the non-H atoms of one Mln$^-$ ion (referred to as Mln-*A*) are located in a single plane, the geometry of the second anion (Mln-*B*) is far from planar (the angle between the mean planes C42—C41—O41—O42 and C42—C43—O43—O44 is 163°). As shown elsewhere (Bauer *et al.*, 2001; Khodov *et al.*, 2014, 2016; Surov *et al.*, 2016), the distorted conformation of the molecule in the condensed phase is an indicator of possible strong interactions involving the displaced atoms, as additional stabilization energy is required to overcome the conformational penalty. In our case, the energy of the hydrogen bonds (including an intramolecular one) and the

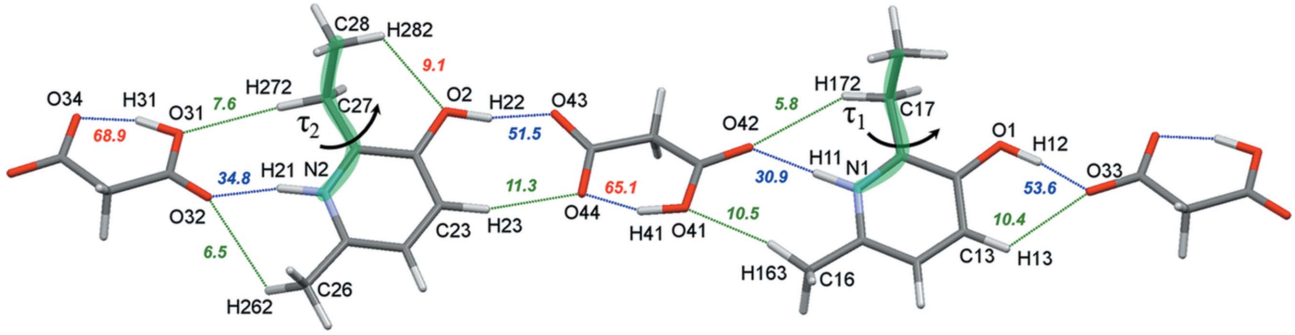

Figure 5
Noncovalent interactions revealed by QTAIMC within the chains of emoxypine and malonate ions in the [EMX+Mln] salt, with the hydrogen bonds shown as blue lines and the main C—H···O contacts shown as green lines. The numbers display the energies of particular noncovalent interactions in kJ mol^{-1}, with red numbers corresponding to the intramolecular contacts.

C—H···O contacts accepted by the O atoms of a single Mln molecule exceeds 100 kJ mol^{-1} (Fig. S1 in the supporting information).

Of the two conformationally different EMX molecules, EMX-*B*, with τ(N1—C1—C6—C7) = 92.6°, participates in a unique intramolecular C28—H282···O2 contact with an energy of 9.6 kJ mol^{-1} (Fig. 5). Since this interaction is absent in the [EMX+Mlt] crystal, where the torsion τ in EMX is only 3° higher, one can suppose the range (93–95°) to be critical for intramolecular C—H···O hydrogen-bond formation.

The strongest interactions in the [EMX+Mln] crystal are two intramolecular hydrogen bonds in conformationally different Mln^{-} ions. Compared to [EMX+Mlt], these interactions are weaker, with the O···O distance equal to 2.44 Å and ρ_b = 0.080–0.086 a.u.; however, they can also be classified as electron-sharing partially covalent interactions (Table 2, and Table S3 in the supporting information).

The energies of synthon interactions are slightly different in conformationally different emoxypine–malonate pairs. For the hydroxy–carboxylate synthon, the total energy is 64 kJ mol^{-1} in the EMX-*A*–Mln-*A* dimer and 63 kJ mol^{-1} in the EMX-*B*–Mln-*B* dimer. Both pyridyl–carboxylate synthons in EMX–Mln are additionally stabilized by two additional C—H···O contacts, with the ethyl group left free to coordinate the molecules of adjacent chains (Fig. 5). The synthon energies in the EMX-*A*–Mln-*B* and EMX-*B*–Mln-*A* dimers are 47 and 49 kJ mol^{-1}, respectively. Note that a weaker hydrogen bond in the considered crystals is always accompanied by stronger C—H···O hydrogen bonds, partially compensating for the difference in synthon energies. Taken together, the interactions within the heterosynthon-bonded chain comprise 55% of all the noncovalent interaction energy in the crystal. Table S3 (see supporting information) contains a detailed description of the metric and quantum–topological properties at the bond critical points.

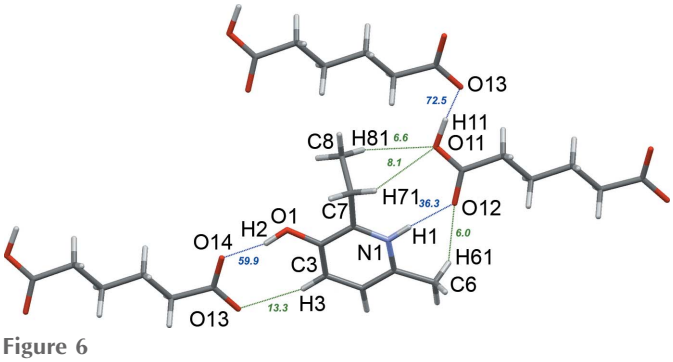

Figure 6
Part of the crystal lattice showing hydrogen bonds (blue lines) and the main C—H···O contacts (green lines) in the [EMX+Adp] salt. The numbers represent the energies of particular noncovalent interactions in kJ mol^{-1}.

The block-like packing of parallel hydrogen-bonded chains shown in Fig. 2(*c*) allows a comparison of the stabilization energy between the chains with different orientations of the ethyl groups (*i.e.* facing towards each other or in opposite directions). It has been found that the stabilization energy of the interactions between the ethyl fragment and its surroundings is compensated by a weakening of other noncovalent interactions, leading to nearly equal contributions to $E_{\rm latt}$.

The total contributions of EMX-*A*, EMX-*B*, Mln-*A* and Mln-*B* to $E_{\rm latt}$ are given in Table S5 (see supporting information). The bent conformation of Mln-*B* is preferable in terms of packing, as it brings an additional 6 kJ mol^{-1} into the lattice energy. A simple single-point calculation of isolated molecules of Mln-*A* and Mln-*B* has revealed that this value is higher than the conformational energy required for bending the malonate ion. The details of this calculation are presented in S3 (see supporting information).

The strongest noncovalent interaction in the [EMX+Adp] crystal, with $E_{\rm int}$ = 72.5 kJ mol^{-1}, is the O11—H11···O13 hydrogen bond linking the Adp^{-} ions into infinite *C*(9) chains along the crystallographic *a* axis. The formation of infinite chains is common in 1:1 salts of dicarboxylic acid, as was reported elsewhere (Surov *et al.*, 2015, 2016).

Each EMX^{+} ion is involved in two hydrogen bonds with Adp^{-}, where it acts as a donor. The hydroxy–carboxylate bond is shorter than the pyridinium–carboxylic bond and has a higher $E_{\rm int}$ value (60 *versus* 36 kJ mol^{-1}). The value of ρ_b = 0.72 a.u. indicates that the O4—H4···O5 hydrogen bond is located in the border region between pure closed-shell interactions and partially covalent bonds. Unlike crystals of pure

Table 4
Thermophysical data for emoxypine salts.

	T_{fus} (salt) (°C) (onset)	ΔH^{T}_{fus} (kJ mol^{-1})^{a}	T_{fus} (acid) (°C)
[EMX+Mln] (1:1)	124.8±0.2	27.4±0.6	135.60
[EMX+Mlt] (1:1)	133.2±0.3	34.8±0.6	142.70
[EMX+Adp] (1:1)	115.8±0.5	53.5±1.1	151.92
EMX	168.81	16.6	–

Note: (*a*) for the salts, the values correspond to a mole of molecules in the asymmetric unit.

EMX, both molecules involved in O—H···*X* hydrogen bonding are located in the same plane. The possible reason for this is the C3—H3···O13 contact with E_{int} equal to 13 kJ mol^{-1}, which stabilizes the hydroxy–carboxylate synthon, making it planar (Fig. 6). The third strongest hydrogen bond in the crystal, with an energy of 36 kJ mol^{-1}, builds the acid–pyridine synthon. This interaction belongs to the 'closed-shell' type, with almost no electron-pair sharing. Surprisingly, the charge-assisted acid–pyridine synthon, with three additional C—H···O contacts, contributes only 57 kJ mol^{-1} to the lattice energy, while the hydroxy–acid synthon brings 73 kJ mol^{-1}. Weaker C—H···O contacts between EMX–EMX and EMX–Adp molecules complete the two-dimensional (2D) hydrogen-bonded sheet. The O atoms are coordinated within heterosynthons in [EMX+Adp] in a fashion similar to that in [EMX+Mlt], with three additional C—H···O contacts for an acid–pyridine hydrogen bond and a stronger single C—H···O contact for a hydroxy–acid hydrogen bond.

A further quantum–topological analysis has revealed a number of weak contacts between adjacent 2D sheets, with the total energy equal to 93 kJ mol^{-1} (about 30% of the total E_{latt} value). Among them, the largest contribution comes from nine C—H···O and C—H···N interactions between the alkyl fragments of the Adp and EMX molecules and free O- and N-atom acceptors, with an average energy of 5 kJ mol^{-1}. Other contributions (about 16 kJ mol^{-1} or 5% each) include phenyl–

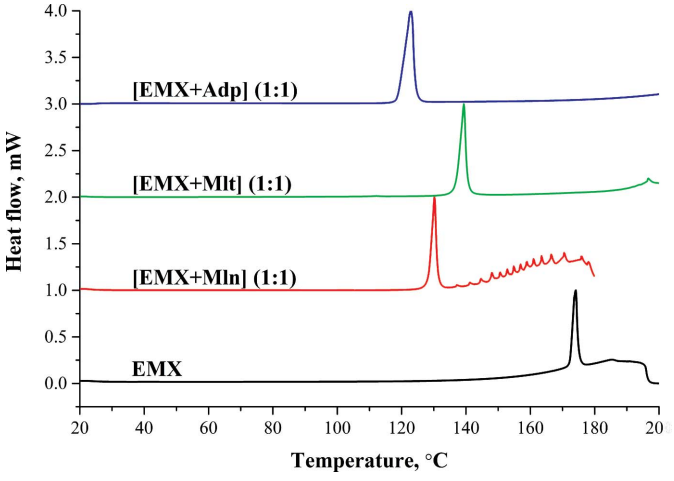

Figure 7
DSC thermograms of EMX, [EMX+Mln], [EMX+Mlt] and [EMX+Adp].

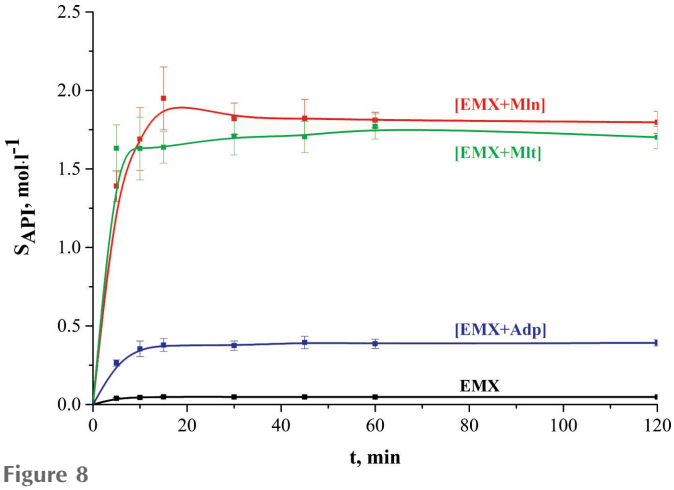

Figure 8
Dissolution profile at 25°C for the salts and pure EMX at pH 7.4.

phenyl and phenyl–carboxyl stacking interactions, and close H···H and C—H···C contacts. A summary of the found bond critical points and metric parameters of the corresponding interactions is presented in Table S4 (see supporting information). The formation of close contacts with the out-of-plane ethyl fragment causes an increase in the interlayer distances in the areas close to the ethyl fragments, leading to a deviation of the layer from planarity.

In contrast to the other two salts studied, the acid–acid interactions in [EMX+Adp] contribute 30% of the lattice energy due to the O11—H11···O13 hydrogen bond and side-to-side C—H···O contacts listed in Table S4 (see supporting information). This packing type is more robust than the chain-like molecular arrangement, as the total interaction energies within the EMX–Adp chain and between the chains are comparable.

Due to strong hydrogen bonds between the anions, [EMX+Adp] has the highest lattice energy of all the studied crystals, *i.e.* 316 kJ mol^{-1} (Table 3). The main bonding patterns, lattice energies and contributions of different types of noncovalent interactions in [EMX+Mlt] and [EMX+Mln] are similar, revealing the packing similarity between these crystals. Therefore, one could expect them to exhibit similar physicochemical properties.

3.3. Thermal analysis

The thermal stability of the emoxypine salts has been evaluated by the DSC (differential scanning calorimetry) method. The DSC results for the salts and pure emoxypine are shown in Fig. 7, and the thermal data are given in Table 4. As Table 4 indicates, the melting temperatures for all of the studied salts are located below the melting temperatures of the respective pure components. The [EMX+Adp] (1:1) salt has the lowest melting temperature (115.8°C), while the largest thermal stability (133.2°C) is observed in [EMX+Mlt] (1:1).

If the main contribution to ΔG of the cocrystal melting process is made by the enthalpy component, we can see a correlation between the temperature [T_{fus} (salt)] and the

Table 5
Solubilities at 25°C for EMX salts and pure EMX in pH 7.4 media.

	Solubility (mol l^{-1})	Solid phase recovered after solubility experiment[a]
[EMX+Mln] (1:1)	1.8±0.1	amorphous
[EMX+Mlt] (1:1)	1.7±0.1	[EMX+Mlt]
[EMX+Adp] (1:1)	0.38±0.05	[EMX+Adp]
EMX	0.047±0.01	EMX

Note: (*a*) the residual materials were identified by DSC and PXRD analyses (Fig. S2–S5 in the supporting information).

melting enthalpy ($\Delta H^{T}_{\rm fus}$) (Perlovich *et al.*, 2013; Perlovich, 2015). In our case, such a correlation is not observed, which allows us to suppose the dominance of the entropy component in the melting process.

It should be mentioned that the melting enthalpy values of the studied salts correlate quantitatively with the crystal lattice energies (see §3.2).

3.4. Aqueous solubility

The main aim of obtaining new cocrystals and salts of an API is to increase solubility. That is why we have studied the emoxypine dissolution processes. The solubility of emoxypine and its salts was examined in a phosphate buffer with pH 7.4 at 25°C. The results of the dissolution experiments for pure EMX and its salts are summarized in Table 5. Fig. 8 shows the dissolution profiles of the salts and EMX in pH 7.4 media.

The solubility of EMX in the pH 7.4 buffer solution is low, reaching 0.047±0.01 mol l^{-1}. As Fig. 8 shows, formation of salts with dicarboxylic acids leads to a significant increase in EMX solubility. The EMX solubility in EMX adipate becomes 8 times higher, while the salts with maleic and malonic acids enhance emoxypine solubility by over 36 times.

It should be said that a solubility increase correlates with the data of the calculated salt crystal lattice energies. The salt of adipic acid with a low crystal lattice energy has the lowest solubility, whereas the salts with maleic and malonic acids with comparable energies increase emoxypine solubility an equal number of times. Besides, the obtained solubility data of the salts confirm the correlation that we established between the carbon chain length of the salts and cocrystals and their solubility parameters. The increased number of carbons in the chain narrows the interval of potential API solubility growth (Manin *et al.*, 2015).

Dissolution profiles for salts and cocrystals usually demonstrate a 'spring and parachute' behaviour (Thakuria *et al.*, 2013; Babu & Nangia, 2011). According to this concept, the 'spring' effect is caused by fast dissociation of the cocrystal to form thermodynamically unstable amorphous-like species of a poorly soluble drug, whereas the longer-term 'parachute' effect occurs because of slow crystallization of this amorphous material to stable crystalline phases in the presence of a well-soluble component. However, the dissolution profiles of EMX salts do not have pronounced 'spring' effects, which are explained by the high stability of the salts in solution. In fact, analysis of the solubility in the bottom phases after the experiment has shown that the [EMX+Mlt] and [EMX+Adp] salts retain the salt form and do not dissociate into individual components.

4. Conclusions

Three new salts of emoxypine with aliphatic dicarboxylic acids (maleic, malonic and adipic acids) were obtained and analyzed by experimental (X-ray and DSC) and theoretical (DFT computations) techniques. Despite the fact that emoxypine is able to form polymorphic salts, as well as salts with different stoichiometric ratios, we found only the anhydrous forms of the considered salts in which the components were in a 1:1 stoichiometric ratio. Alternation of the orientation of the anions was observed in the chains of the emoxypine malonate and maleate salts, while the orientation of the EMX ions changes only in [EMX+Mlt]. It was found that the absence of an intramolecular hydrogen bond in the adipate anion led to a higher lattice energy and, consequently, lower solubility and higher fusion enthalpy. Thermal analysis of the EMX salts showed that the values of the melting enthalpies of the studied salts correlated quantitatively with the values of the crystal lattice energies. The solubility of the salts was measured in a pharmaceutically relevant buffer solution with pH 7.4. The [EMX+Mlt], [EMX+Mln] and [EMX+Adp] salts demonstrated a 36-, 38- and 8-fold solubility improvement, respectively, relative to pure EMX. Further biopharmaceutical studies are required to investigate and to compare the behaviour of the salts *in vivo*.

Acknowledgements

DSC and PXRD experiments were conducted using the equipment of the centre for joint use of scientific equipment 'The upper Volga region centre of physicochemical research'.

Funding information

Funding for this research was provided by: Russian Science Foundation (grant No. 17-73-10351).

References

Abramov, Y. A. (2015). *Mol. Pharm.* **12**, 2126–2141.
Babu, N. J. & Nangia, A. (2011). *Cryst. Growth Des.* **11**, 2662–2679.
Bansal, A. K., Kumar, L. & Amin, A. (2008). *Pharm. Technol.* **3**, 32, http://www.pharmtech.com/salt-selection-drug-development (accessed 2 April 2018).
Basavoju, S., Boström, D. & Velaga, S. P. (2006). *Cryst. Growth Des.* **6**, 2699–2708.
Bauer, J., Spanton, S., Henry, R., Quick, J., Dziki, W., Porter, W. & Morris, J. (2001). *Pharm. Res.* **18**, 859–866.
Borovikov, V. E. (2016). Patent RU2605825.
Bruker (2008). *APEX2*, *SAINT* and *SADABS*. Bruker AXS Inc., Madison, Wisconsin, USA.
Bruni, G., Maietta, M., Scotti, F., Maggi, L., Bini, M., Ferrari, S., Capsoni, D., Boiocchi, M., Berbenni, V., Milanese, C., Girella, A. & Marini, A. (2013). *Acta Cryst.* B**69**, 362–370.
Chemicalize (2018). *Chemicalize* web applet, March 2018, https://chemicalize.com/, developed by ChemAxon (http://www.chemaxon.com).

Chernyshev, V. V., Efimov, S. Y., Paseshnichenko, K. A. & Shiryaev, A. A. (2013). *Acta Cryst.* C**69**, 1549–1552.
Chesnokova, N. B., Beznos, O. V., Pavlenko, T. A., Zabozlaev, A. A. & Pavlova, M. V. (2015). *Bull. Exp. Biol. Med.* **158**, 346–348.
Cruz-Cabeza, A. J. (2012). *CrystEngComm*, **14**, 6362–6365.
Dominiak, P., Espinosa, E. & Angyan, J. (2012). *Modern Charge Density Analysis*, edited by C. Gatti & P. Macchi, pp. 387–433. Berlin: Springer Science & Business Media.
Dovesi, R., Orlando, R., Erba, A., Zicovich-Wilson, C. M., Civalleri, B., Casassa, S., Maschio, L., Ferrabone, M., De La Pierre, M., D'Arco, P., Noël, Y., Causà, M., Rérat, M. & Kirtman, B. (2014). *Int. J. Quantum Chem.* **114**, 1287–1317.
Etter, C. (1990). *Acc. Chem. Res.* **23**, 120–126.
Gatti, C. (2005). *Z. Kristallogr.* **220**, 399–457.
Gatti, C., Saunders, V. R. & Roetti, C. (1994). *J. Chem. Phys.* **101**, 10686–10696.
Grimme, S. J. (2006). *J. Comput. Chem.* **27**, 1787–1799.
Khodov, I. A., Efimov, S. V., Klochkov, V. V., Alper, G. A. & Batista de Carvalho, L. A. E. (2014). *Eur. J. Pharm. Sci.* **65**, 64–73.
Khodov, I. A., Efimov, S. V., Klochkov, V. V., Batista de Carvalho, L. A. E. & Kiselev, M. G. (2016). *J. Mol. Struct.* **1106**, 373–381.
Levitskaya, O. V., Syroeshkin, A. V. & Pleteneva, T. V. (2016). *Pharm. Chem. J.* **49**, 779–781.
Lyakhov, A. S., Ivashkevich, L. S., Survilo, V. L., Kipnis, A. M. & Trukhachova, T. V. (2012*b*). *Acta Cryst.* C**68**, o365–o368.
Lyakhov, A. S., Ivashkevich, L. S., Survilo, V. L. & Trukhachova, T. V. (2012*a*). *Acta Cryst.* C**68**, o33–o36.
Manin, A. N., Surov, A. O., Churakov, A. V. & Perlovich, G. L. (2015). *Crystals*, **5**, 650–669.
Mata, I., Alkorta, I., Espinosa, E. & Molins, E. (2011). *Chem. Phys. Lett.* **507**, 185–189.
Pascale, F., Zicovich-Wilson, C. M., Gejo, F. L., Civalleri, B., Orlando, R. & Dovesi, R. (2004). *J. Comp. Chem.* **25**, 888–897.
Paulekuhn, G. S., Dressman, J. B. & Saal, C. (2007). *J. Med. Chem.* **50**, 6665–6672.
Perlovich, G. L. (2014). *Mol. Pharm.* **11**, 1–11.
Perlovich, G. L. (2015). *CrystEngComm*, **17**, 7019–7028.
Perlovich, G. L., Ryzhakov, A. M., Tkachev, V. V., Hansen, L. K., Raevsky, O. A. (2013). *Cryst. Growth Des.* **13**, 4002–4016.
Pudipeddi, M., Serajuddin, A. T. M., Grant, D. J. W. & Stahl, P. (2002). *Handbook of Pharmaceutical Salts, Properties, Selection and Use*, edited by P. H. Stahl & C. G. Wermuth, pp. 19–40. Weinheim: Wiley-VCH.
Sheldrick, G. M. (2008). *Acta Cryst.* A**64**, 112–122.
Steiner, T. (2002). *Angew. Chem. Int. Ed.* **41**, 48–76.
Surov, A. O., Manin, A. N., Voronin, A. P., Drozd, K. V., Simagina, A. A., Churakov, A. V. & Perlovich, G. L. (2015). *Eur. J. Pharm. Sci.* **77**, 112–121.
Surov, A. O., Voronin, A. P., Simagina, A. A., Churakov, A. V. & Perlovich, G. L. (2016). *Cryst. Growth Des.* **16**, 2605–2617.
Thakuria, R., Delori, A., Jones, W., Lipert, M. P., Roy, L. & Rodríguez-Hornedo, N. (2013). *Int. J. Pharm.* **453**, 101–125.
Vener, M. V., Levina, E. O., Koloskov, O. A., Rykounov, A. A., Voronin, A. P. & Tsirelson, V. G. (2014). *Cryst. Growth Des.* **14**, 4997–5003.
Voronin, A. P., Perlovich, G. L. & Vener, M. V. (2016). *Comput. Theor. Chem.* **1092**, 1–11.
Yasnetsov, V. V., Skachilova, S. Y., Sernov, L. N., Voronina, T. A., Yasnetsov, V. V. & Zhurnal, T. K. (2012). *Pharm. Chem. J.* **46**, 199–202.
Yasnetsov, V. V., Skachilova, S. Y., Voronina, T. A. & Yasnetsov, V. V. (2010). Patent RU2394816. (In Russian.)

supporting information

Acta Cryst. (2018). C**74** [https://doi.org/10.1107/S2053229618007386]

Pharmaceutical salts of emoxypine with dicarboxylic acids

Alex N. Manin, Alexander P. Voronin, Ksenia V. Drozd, Andrei V. Churakov and German L. Perlovich

Computing details

For all structures, data collection: *APEX2* (Bruker, 2008); cell refinement: *SAINT* (Bruker, 2008); data reduction: *SAINT* (Bruker, 2008); program(s) used to solve structure: *SHELXTL* (Sheldrick, 2008); program(s) used to refine structure: *SHELXTL* (Sheldrick, 2008); molecular graphics: *SHELXTL* (Sheldrick, 2008); software used to prepare material for publication: *SHELXTL* (Sheldrick, 2008).

2-Ethyl-3-hydroxy-6-methylpyridin-1-ium 3-carboxyprop-2-enoate (I)

Crystal data

$C_8H_{12}NO^+·C_4H_3O_4^-$
M_r = 253.25
Orthorhombic, *Pccn*
Hall symbol: -P 2ab 2ac
a = 26.571 (3) Å
b = 6.9074 (8) Å
c = 13.5152 (16) Å
V = 2480.6 (5) Å^3
Z = 8
F(000) = 1072
D_x = 1.356 Mg m^{-3}
Mo *Kα* radiation, *λ* = 0.71073 Å
Cell parameters from 6269 reflections
θ = 3.0–30.1°
μ = 0.11 mm^{-1}
T = 150 K
Parallelepiped, colourless
0.35 × 0.20 × 0.20 mm

Data collection

Bruker SMART APEXII diffractometer
Radiation source: fine-focus sealed tube
Graphite monochromator
ω scans
Absorption correction: multi-scan (SADABS; Bruker, 2008)
T_{min} = 0.964, T_{max} = 0.979
19445 measured reflections
2713 independent reflections
2282 reflections with $I > 2\sigma(I)$
R_{int} = 0.026
θ_{max} = 27.0°, θ_{min} = 3.0°
h = −33→33
k = −8→8
l = −17→16

Refinement

Refinement on F^2
Least-squares matrix: full
$R[F^2 > 2\sigma(F^2)]$ = 0.037
$wR(F^2)$ = 0.101
S = 1.04
2713 reflections
223 parameters
0 restraints
Primary atom site location: structure-invariant direct methods
Secondary atom site location: difference Fourier map
Hydrogen site location: difference Fourier map
All H-atom parameters refined
$w = 1/[\sigma^2(F_o^2) + (0.0506P)^2 + 0.7672P]$ where $P = (F_o^2 + 2F_c^2)/3$
$(\Delta/\sigma)_{max} < 0.001$
$\Delta\rho_{max}$ = 0.23 e Å^{-3}
$\Delta\rho_{min}$ = −0.19 e Å^{-3}

Special details

Geometry. All esds (except the esd in the dihedral angle between two l.s. planes) are estimated using the full covariance matrix. The cell esds are taken into account individually in the estimation of esds in distances, angles and torsion angles; correlations between esds in cell parameters are only used when they are defined by crystal symmetry. An approximate (isotropic) treatment of cell esds is used for estimating esds involving l.s. planes.

Refinement. Refinement of F^2 against ALL reflections. The weighted R-factor wR and goodness of fit S are based on F^2, conventional R-factors R are based on F, with F set to zero for negative F^2. The threshold expression of $F^2 > 2\text{sigma}(F^2)$ is used only for calculating R-factors(gt) etc. and is not relevant to the choice of reflections for refinement. R-factors based on F^2 are statistically about twice as large as those based on F, and R- factors based on ALL data will be even larger.

Fractional atomic coordinates and isotropic or equivalent isotropic displacement parameters (Å²)

	x	*y*	*z*	U_{iso}*/U_{eq}
O1	0.23337 (3)	0.51028 (14)	0.25508 (7)	0.0328 (2)
H2	0.2066 (8)	0.492 (3)	0.2909 (13)	0.057 (5)*
N1	0.36097 (4)	0.57375 (14)	0.32811 (8)	0.0253 (2)
H1	0.3918 (6)	0.588 (2)	0.2955 (11)	0.037 (4)*
C1	0.31985 (4)	0.56061 (17)	0.27019 (9)	0.0246 (3)
C2	0.27330 (4)	0.52561 (17)	0.31535 (9)	0.0257 (3)
C3	0.27151 (5)	0.51191 (18)	0.41811 (9)	0.0294 (3)
C4	0.31499 (5)	0.53136 (18)	0.47344 (9)	0.0293 (3)
C5	0.36080 (5)	0.56154 (17)	0.42794 (9)	0.0276 (3)
C6	0.41005 (6)	0.5867 (3)	0.48088 (11)	0.0394 (3)
C7	0.32582 (5)	0.5779 (2)	0.16069 (9)	0.0293 (3)
C8	0.32970 (6)	0.3791 (2)	0.11233 (10)	0.0412 (4)
H3	0.2400 (6)	0.488 (2)	0.4490 (11)	0.033 (4)*
H4	0.3130 (6)	0.524 (2)	0.5448 (12)	0.039 (4)*
H61	0.4111 (8)	0.505 (3)	0.5358 (18)	0.079 (7)*
H62	0.4123 (8)	0.718 (3)	0.5043 (16)	0.085 (7)*
H63	0.4384 (7)	0.563 (3)	0.4393 (15)	0.060 (5)*
H71	0.3554 (6)	0.659 (2)	0.1477 (11)	0.037 (4)*
H72	0.2954 (6)	0.648 (2)	0.1362 (11)	0.039 (4)*
H81	0.2974 (7)	0.301 (3)	0.1274 (12)	0.059 (5)*
H82	0.3334 (6)	0.391 (3)	0.0408 (13)	0.049 (5)*
H83	0.3600 (6)	0.312 (2)	0.1389 (12)	0.049 (5)*
O11	0.51272 (4)	0.55390 (18)	0.29968 (7)	0.0456 (3)
H11	0.5546 (9)	0.540 (3)	0.2876 (16)	0.083 (7)*
O12	0.44379 (3)	0.59189 (18)	0.21062 (8)	0.0479 (3)
O13	0.65378 (3)	0.55089 (16)	0.14008 (7)	0.0394 (3)
O14	0.60222 (4)	0.52160 (17)	0.26715 (7)	0.0422 (3)
C11	0.48987 (5)	0.5836 (2)	0.21751 (10)	0.0329 (3)
C12	0.51939 (5)	0.6098 (2)	0.12445 (10)	0.0371 (3)
C13	0.56863 (5)	0.5967 (2)	0.10733 (10)	0.0338 (3)
C14	0.61100 (4)	0.55363 (18)	0.17691 (9)	0.0265 (3)
H12	0.4980 (6)	0.642 (2)	0.0678 (12)	0.046 (4)*
H13	0.5794 (6)	0.614 (2)	0.0406 (12)	0.041 (4)*

Atomic displacement parameters (Å²)

	U^{11}	U^{22}	U^{33}	U^{12}	U^{13}	U^{23}
O1	0.0171 (4)	0.0484 (6)	0.0329 (5)	−0.0021 (4)	0.0017 (3)	0.0017 (4)
N1	0.0185 (5)	0.0295 (5)	0.0279 (5)	−0.0003 (4)	0.0020 (4)	0.0006 (4)
C1	0.0201 (5)	0.0265 (6)	0.0271 (6)	0.0005 (4)	0.0016 (4)	0.0014 (4)
C2	0.0191 (5)	0.0273 (6)	0.0308 (6)	0.0007 (4)	0.0019 (4)	0.0007 (5)
C3	0.0254 (6)	0.0306 (6)	0.0320 (7)	−0.0009 (5)	0.0092 (5)	0.0004 (5)
C4	0.0328 (6)	0.0305 (6)	0.0247 (6)	0.0005 (5)	0.0037 (5)	−0.0003 (5)
C5	0.0281 (6)	0.0280 (6)	0.0268 (6)	0.0005 (5)	−0.0013 (5)	−0.0028 (5)
C6	0.0315 (7)	0.0538 (9)	0.0329 (7)	−0.0023 (6)	−0.0064 (6)	−0.0047 (7)
C7	0.0201 (6)	0.0413 (7)	0.0264 (6)	−0.0001 (5)	0.0021 (4)	0.0078 (5)
C8	0.0424 (8)	0.0549 (9)	0.0262 (7)	0.0094 (7)	0.0031 (6)	−0.0026 (6)
O11	0.0258 (5)	0.0780 (8)	0.0329 (5)	0.0000 (5)	0.0072 (4)	0.0056 (5)
O12	0.0184 (5)	0.0698 (8)	0.0557 (7)	0.0039 (4)	0.0079 (4)	0.0079 (6)
O13	0.0173 (4)	0.0647 (7)	0.0363 (5)	0.0045 (4)	0.0007 (4)	0.0083 (5)
O14	0.0233 (5)	0.0745 (8)	0.0287 (5)	−0.0030 (5)	−0.0019 (3)	0.0090 (5)
C11	0.0213 (6)	0.0386 (7)	0.0388 (7)	0.0008 (5)	0.0057 (5)	0.0011 (6)
C12	0.0209 (6)	0.0590 (9)	0.0315 (7)	0.0058 (6)	−0.0019 (5)	0.0045 (6)
C13	0.0231 (6)	0.0527 (8)	0.0256 (6)	0.0042 (6)	0.0007 (5)	0.0053 (6)
C14	0.0192 (5)	0.0308 (6)	0.0296 (6)	−0.0004 (4)	−0.0015 (4)	0.0017 (5)

Geometric parameters (Å, º)

O1—C2	1.3419 (14)	C7—C8	1.524 (2)
O1—H2	0.87 (2)	C7—H71	0.979 (15)
N1—C1	1.3471 (15)	C7—H72	0.999 (16)
N1—C5	1.3519 (16)	C8—H81	1.035 (18)
N1—H1	0.936 (16)	C8—H82	0.976 (18)
C1—C2	1.4004 (16)	C8—H83	0.995 (17)
C1—C7	1.4932 (17)	O11—C11	1.2821 (16)
C2—C3	1.3928 (18)	O11—H11	1.13 (2)
C3—C4	1.3827 (18)	O12—C11	1.2294 (16)
C3—H3	0.951 (15)	O13—C14	1.2412 (15)
C4—C5	1.3795 (17)	O14—C14	1.2612 (16)
C4—H4	0.968 (16)	C11—C12	1.4932 (18)
C5—C6	1.5014 (18)	C12—C13	1.3318 (18)
C6—H61	0.94 (2)	C12—H12	0.981 (16)
C6—H62	0.96 (2)	C13—C14	1.4967 (17)
C6—H63	0.95 (2)	C13—H13	0.954 (16)
C2—O1—H2	108.7 (12)	C1—C7—H71	107.9 (9)
C1—N1—C5	124.96 (10)	C8—C7—H71	112.5 (9)
C1—N1—H1	116.4 (9)	C1—C7—H72	106.3 (8)
C5—N1—H1	118.6 (9)	C8—C7—H72	110.5 (9)
N1—C1—C2	118.34 (11)	H71—C7—H72	108.2 (13)
N1—C1—C7	118.97 (10)	C7—C8—H81	109.4 (10)
C2—C1—C7	122.66 (11)	C7—C8—H82	110.7 (10)

O1—C2—C3	124.96 (11)	H81—C8—H82	108.9 (13)
O1—C2—C1	116.58 (11)	C7—C8—H83	108.6 (10)
C3—C2—C1	118.45 (11)	H81—C8—H83	110.8 (14)
C4—C3—C2	120.28 (11)	H82—C8—H83	108.4 (13)
C4—C3—H3	121.1 (9)	C11—O11—H11	110.8 (11)
C2—C3—H3	118.6 (9)	C14—O14—H11	111.6 (9)
C5—C4—C3	120.72 (11)	O12—C11—O11	123.00 (12)
C5—C4—H4	120.0 (9)	O12—C11—C12	116.98 (12)
C3—C4—H4	119.3 (9)	O11—C11—C12	120.02 (11)
N1—C5—C4	117.21 (11)	C13—C12—C11	130.85 (12)
N1—C5—C6	117.73 (11)	C13—C12—H12	116.7 (9)
C4—C5—C6	125.04 (12)	C11—C12—H12	112.4 (9)
C5—C6—H61	109.6 (14)	C12—C13—C14	130.03 (12)
C5—C6—H62	108.7 (13)	C12—C13—H13	116.9 (9)
H61—C6—H62	107.9 (18)	C14—C13—H13	113.1 (9)
C5—C6—H63	112.8 (12)	O13—C14—O14	123.67 (11)
H61—C6—H63	109.9 (17)	O13—C14—C13	116.10 (11)
H62—C6—H63	107.8 (16)	O14—C14—C13	120.23 (11)
C1—C7—C8	111.12 (11)		

C5—N1—C1—C2	−2.13 (18)	C1—N1—C5—C6	−177.81 (12)
C5—N1—C1—C7	179.69 (12)	C3—C4—C5—N1	0.90 (18)
N1—C1—C2—O1	−178.93 (10)	C3—C4—C5—C6	179.29 (13)
C7—C1—C2—O1	−0.81 (18)	N1—C1—C7—C8	95.66 (14)
N1—C1—C2—C3	1.91 (17)	C2—C1—C7—C8	−82.44 (15)
C7—C1—C2—C3	−179.97 (12)	O12—C11—C12—C13	−175.27 (16)
O1—C2—C3—C4	−179.51 (12)	O11—C11—C12—C13	4.6 (3)
C1—C2—C3—C4	−0.43 (19)	C11—C12—C13—C14	−1.0 (3)
C2—C3—C4—C5	−1.00 (19)	C12—C13—C14—O13	−179.87 (16)
C1—N1—C5—C4	0.70 (18)	C12—C13—C14—O14	0.5 (2)

Hydrogen-bond geometry (Å, º)

D—H···*A*	*D*—H	H···*A*	*D*···*A*	*D*—H···*A*
O11—H11···O14	1.13 (2)	1.30 (2)	2.4288 (14)	176 (2)
O1—H2···O13^{i}	0.87 (2)	1.71 (2)	2.5804 (13)	178.5 (19)
N1—H1···O12	0.936 (16)	1.795 (17)	2.7165 (14)	167.5 (14)

Symmetry code: (i) $x-1/2, -y+1, -z+1/2$.

2-Ethyl-3-hydroxy-6-methylpyridin-1-ium 3-carboxypropanoate (II)

Crystal data

$C_8H_{12}NO^+·C_3H_3O_4^-$
M_r = 241.24
Triclinic, $P\overline{1}$
Hall symbol: -P 1
a = 8.9211 (7) Å
b = 10.5301 (8) Å
c = 13.7175 (10) Å
α = 80.0535 (11)°
β = 86.3313 (11)°
γ = 66.5117 (10)°
V = 1164.07 (15) Å^3
Z = 4
F(000) = 512
D_x = 1.377 Mg m^{-3}

Mo $K\alpha$ radiation, λ = 0.71073 Å
Cell parameters from 5243 reflections
θ = 2.5–30.6°
μ = 0.11 mm^{-1}
T = 150 K
Prism, colourless
0.40 × 0.20 × 0.05 mm

Data collection

Bruker SMART APEXII diffractometer
Radiation source: fine-focus sealed tube
Graphite monochromator
ω scans
Absorption correction: multi-scan (SADABS; Bruker, 2008)
T_{min} = 0.958, T_{max} = 0.995
12144 measured reflections
5599 independent reflections
4307 reflections with $I > 2\sigma(I)$
R_{int} = 0.020
θ_{max} = 28.0°, θ_{min} = 2.4°
h = −11→11
k = −13→13
l = −18→18

Refinement

Refinement on F^2
Least-squares matrix: full
$R[F^2 > 2\sigma(F^2)]$ = 0.039
$wR(F^2)$ = 0.108
S = 1.03
5599 reflections
427 parameters
0 restraints
Primary atom site location: structure-invariant direct methods
Secondary atom site location: difference Fourier map
Hydrogen site location: difference Fourier map
All H-atom parameters refined
$w = 1/[\sigma^2(F_o^2) + (0.0632P)^2 + 0.1019P]$ where $P = (F_o^2 + 2F_c^2)/3$
$(\Delta/\sigma)_{max} < 0.001$
$\Delta\rho_{max}$ = 0.33 e Å^{-3}
$\Delta\rho_{min}$ = −0.23 e Å^{-3}

Special details

Geometry. All esds (except the esd in the dihedral angle between two l.s. planes) are estimated using the full covariance matrix. The cell esds are taken into account individually in the estimation of esds in distances, angles and torsion angles; correlations between esds in cell parameters are only used when they are defined by crystal symmetry. An approximate (isotropic) treatment of cell esds is used for estimating esds involving l.s. planes.

Refinement. Refinement of F^2 against ALL reflections. The weighted R-factor wR and goodness of fit S are based on F^2, conventional R-factors R are based on F, with F set to zero for negative F^2. The threshold expression of $F^2 > 2\text{sigma}(F^2)$ is used only for calculating R-factors(gt) etc. and is not relevant to the choice of reflections for refinement. R-factors based on F^2 are statistically about twice as large as those based on F, and R- factors based on ALL data will be even larger.

Fractional atomic coordinates and isotropic or equivalent isotropic displacement parameters (Å²)

	x	y	z	U_{iso}*/U_{eq}
O1	0.25059 (11)	0.94822 (10)	0.49431 (6)	0.0303 (2)
H12	0.324 (2)	0.866 (2)	0.4794 (13)	0.053 (5)*
N1	0.27799 (11)	1.14462 (10)	0.67428 (7)	0.0191 (2)
H11	0.2147 (18)	1.2292 (16)	0.6934 (11)	0.032 (4)*
C11	0.21972 (13)	1.11105 (12)	0.59834 (8)	0.0194 (2)
C12	0.31050 (14)	0.98134 (12)	0.56914 (8)	0.0210 (2)
C13	0.45557 (14)	0.89267 (12)	0.61915 (9)	0.0225 (2)
C14	0.50934 (14)	0.93460 (13)	0.69542 (9)	0.0228 (2)
C15	0.41919 (14)	1.06403 (12)	0.72318 (8)	0.0210 (2)
C16	0.46939 (17)	1.11937 (15)	0.80301 (10)	0.0278 (3)
C17	0.06539 (14)	1.21647 (13)	0.54769 (9)	0.0253 (3)
C18	0.10265 (19)	1.30767 (18)	0.45902 (12)	0.0439 (4)

H13	0.5167 (17)	0.8008 (15)	0.5993 (10)	0.028 (4)*
H14	0.6073 (17)	0.8775 (14)	0.7317 (10)	0.024 (3)*
H161	0.496 (2)	1.055 (2)	0.8627 (15)	0.064 (6)*
H162	0.568 (3)	1.137 (2)	0.7861 (14)	0.071 (6)*
H163	0.388 (2)	1.202 (2)	0.8186 (14)	0.062 (6)*
H171	0.0018 (18)	1.1681 (16)	0.5262 (11)	0.036 (4)*
H172	−0.0015 (18)	1.2712 (16)	0.5950 (11)	0.037 (4)*
H181	0.173 (2)	1.245 (2)	0.4109 (15)	0.068 (6)*
H182	0.001 (2)	1.3805 (19)	0.4255 (13)	0.057 (5)*
H183	0.156 (2)	1.3620 (19)	0.4801 (14)	0.059 (5)*
N2	0.83343 (12)	0.11657 (10)	0.17789 (7)	0.0205 (2)
H21	0.7931 (19)	0.1931 (17)	0.2111 (12)	0.039 (4)*
O2	0.71557 (11)	−0.00878 (9)	−0.01610 (6)	0.0281 (2)
H22	0.759 (2)	−0.092 (2)	−0.0455 (15)	0.068 (6)*
C21	0.74586 (14)	0.11303 (12)	0.10278 (8)	0.0206 (2)
C22	0.80482 (14)	−0.00756 (12)	0.05829 (8)	0.0205 (2)
C23	0.94858 (14)	−0.11854 (12)	0.09343 (9)	0.0222 (2)
C24	1.03252 (14)	−0.10822 (13)	0.17156 (9)	0.0224 (2)
C25	0.97484 (13)	0.01199 (12)	0.21409 (8)	0.0208 (2)
C26	1.05829 (16)	0.03354 (15)	0.29668 (10)	0.0282 (3)
C27	0.59039 (15)	0.23649 (13)	0.07126 (9)	0.0269 (3)
C28	0.60503 (18)	0.32019 (14)	−0.02888 (10)	0.0326 (3)
H23	0.9861 (16)	−0.2020 (14)	0.0647 (9)	0.020 (3)*
H24	1.1283 (17)	−0.1833 (15)	0.1985 (10)	0.027 (4)*
H261	1.107 (2)	0.1014 (19)	0.2734 (13)	0.056 (5)*
H262	0.985 (2)	0.0716 (18)	0.3475 (13)	0.047 (5)*
H263	1.142 (2)	−0.058 (2)	0.3272 (13)	0.059 (5)*
H271	0.502 (2)	0.2003 (17)	0.0657 (12)	0.043 (4)*
H272	0.5614 (17)	0.2958 (15)	0.1213 (11)	0.031 (4)*
H281	0.498 (2)	0.3990 (17)	−0.0499 (12)	0.046 (4)*
H282	0.6397 (18)	0.2554 (16)	−0.0781 (11)	0.037 (4)*
H283	0.688 (2)	0.3614 (18)	−0.0290 (13)	0.052 (5)*
O31	0.47446 (13)	0.44831 (11)	0.27092 (8)	0.0418 (3)
H31	0.393 (3)	0.539 (2)	0.3028 (16)	0.087 (7)*
O32	0.74168 (13)	0.32588 (10)	0.28866 (8)	0.0410 (3)
O33	0.47330 (12)	0.71824 (10)	0.44915 (7)	0.0385 (2)
O34	0.33650 (12)	0.65525 (11)	0.35028 (8)	0.0406 (3)
C31	0.61609 (17)	0.42311 (13)	0.30669 (9)	0.0283 (3)
C32	0.62348 (16)	0.51936 (13)	0.37450 (10)	0.0254 (3)
C33	0.46522 (16)	0.64055 (13)	0.39291 (9)	0.0267 (3)
H321	0.6670 (19)	0.4621 (16)	0.4395 (12)	0.038 (4)*
H322	0.6975 (19)	0.5572 (16)	0.3481 (11)	0.036 (4)*
O41	1.18702 (11)	−0.57232 (10)	−0.14240 (8)	0.0366 (2)
H41	1.147 (3)	−0.493 (2)	−0.0999 (16)	0.084 (7)*
O42	1.06394 (11)	−0.61278 (9)	−0.26157 (7)	0.0320 (2)
O43	0.79442 (11)	−0.21875 (9)	−0.10746 (7)	0.0324 (2)
O44	1.04830 (11)	−0.36617 (10)	−0.06211 (7)	0.0340 (2)
C41	1.06034 (15)	−0.54701 (12)	−0.19505 (9)	0.0241 (3)

C42	0.90252 (16)	−0.43260 (14)	−0.17060 (11)	0.0294 (3)
C43	0.91565 (15)	−0.33013 (12)	−0.10873 (8)	0.0239 (3)
H421	0.842 (2)	−0.3832 (19)	−0.2290 (14)	0.059 (5)*
H422	0.838 (2)	−0.4797 (19)	−0.1307 (13)	0.056 (5)*

Atomic displacement parameters (Å²)

	U^{11}	U^{22}	U^{33}	U^{12}	U^{13}	U^{23}
O1	0.0282 (5)	0.0316 (5)	0.0297 (5)	−0.0040 (4)	−0.0066 (4)	−0.0182 (4)
N1	0.0195 (5)	0.0172 (5)	0.0195 (5)	−0.0047 (4)	−0.0006 (4)	−0.0065 (4)
C11	0.0184 (5)	0.0208 (6)	0.0184 (5)	−0.0064 (4)	−0.0001 (4)	−0.0048 (4)
C12	0.0208 (5)	0.0228 (6)	0.0199 (5)	−0.0074 (5)	0.0005 (4)	−0.0080 (4)
C13	0.0217 (6)	0.0191 (6)	0.0249 (6)	−0.0048 (5)	0.0016 (4)	−0.0078 (5)
C14	0.0199 (6)	0.0221 (6)	0.0239 (6)	−0.0051 (5)	−0.0032 (4)	−0.0035 (5)
C15	0.0213 (5)	0.0227 (6)	0.0197 (5)	−0.0090 (5)	−0.0022 (4)	−0.0035 (4)
C16	0.0290 (7)	0.0287 (7)	0.0260 (6)	−0.0090 (5)	−0.0077 (5)	−0.0086 (5)
C17	0.0197 (6)	0.0265 (6)	0.0254 (6)	−0.0015 (5)	−0.0048 (5)	−0.0097 (5)
C18	0.0335 (8)	0.0404 (9)	0.0431 (9)	−0.0044 (7)	−0.0106 (7)	0.0096 (7)
N2	0.0216 (5)	0.0201 (5)	0.0209 (5)	−0.0073 (4)	0.0003 (4)	−0.0082 (4)
O2	0.0281 (5)	0.0272 (5)	0.0280 (4)	−0.0051 (4)	−0.0080 (4)	−0.0133 (4)
C21	0.0199 (5)	0.0218 (6)	0.0202 (5)	−0.0069 (4)	0.0000 (4)	−0.0068 (4)
C22	0.0214 (5)	0.0214 (6)	0.0194 (5)	−0.0076 (5)	−0.0005 (4)	−0.0071 (4)
C23	0.0243 (6)	0.0187 (6)	0.0230 (6)	−0.0064 (5)	0.0013 (4)	−0.0070 (4)
C24	0.0204 (6)	0.0223 (6)	0.0216 (5)	−0.0049 (5)	−0.0016 (4)	−0.0036 (4)
C25	0.0199 (5)	0.0240 (6)	0.0194 (5)	−0.0090 (5)	−0.0002 (4)	−0.0046 (4)
C26	0.0274 (6)	0.0337 (7)	0.0255 (6)	−0.0120 (6)	−0.0055 (5)	−0.0083 (5)
C27	0.0218 (6)	0.0239 (6)	0.0306 (6)	−0.0008 (5)	−0.0031 (5)	−0.0124 (5)
C28	0.0317 (7)	0.0248 (7)	0.0349 (7)	−0.0030 (6)	−0.0072 (6)	−0.0058 (6)
O31	0.0443 (6)	0.0359 (6)	0.0473 (6)	−0.0107 (5)	−0.0108 (5)	−0.0211 (5)
O32	0.0459 (6)	0.0291 (5)	0.0450 (6)	−0.0050 (4)	0.0010 (5)	−0.0229 (4)
O33	0.0390 (5)	0.0326 (5)	0.0442 (6)	−0.0073 (4)	0.0044 (4)	−0.0253 (4)
O34	0.0287 (5)	0.0366 (6)	0.0541 (6)	−0.0048 (4)	−0.0041 (4)	−0.0193 (5)
C31	0.0392 (7)	0.0212 (6)	0.0251 (6)	−0.0110 (5)	0.0018 (5)	−0.0084 (5)
C32	0.0272 (6)	0.0232 (6)	0.0275 (6)	−0.0094 (5)	0.0046 (5)	−0.0115 (5)
C33	0.0300 (6)	0.0227 (6)	0.0274 (6)	−0.0093 (5)	0.0060 (5)	−0.0088 (5)
O41	0.0276 (5)	0.0338 (5)	0.0433 (5)	−0.0010 (4)	−0.0053 (4)	−0.0185 (4)
O42	0.0382 (5)	0.0233 (5)	0.0330 (5)	−0.0068 (4)	0.0004 (4)	−0.0140 (4)
O43	0.0335 (5)	0.0265 (5)	0.0354 (5)	−0.0044 (4)	−0.0047 (4)	−0.0164 (4)
O44	0.0295 (5)	0.0362 (5)	0.0374 (5)	−0.0084 (4)	−0.0067 (4)	−0.0175 (4)
C41	0.0292 (6)	0.0177 (5)	0.0246 (6)	−0.0083 (5)	0.0018 (5)	−0.0048 (5)
C42	0.0276 (7)	0.0257 (6)	0.0333 (7)	−0.0041 (5)	−0.0049 (5)	−0.0147 (5)
C43	0.0286 (6)	0.0234 (6)	0.0212 (6)	−0.0106 (5)	0.0014 (5)	−0.0069 (5)

Geometric parameters (Å, º)

O1—C12	1.3430 (13)	C23—H23	0.953 (14)
O1—H12	0.901 (19)	C24—C25	1.3802 (16)
N1—C15	1.3477 (15)	C24—H24	0.945 (14)

N1—C11	1.3504 (14)	C25—C26	1.4902 (16)
N1—H11	0.918 (15)	C26—H261	0.979 (18)
C11—C12	1.3956 (16)	C26—H262	0.950 (17)
C11—C17	1.4994 (16)	C26—H263	0.991 (18)
C12—C13	1.3951 (16)	C27—C28	1.527 (2)
C13—C14	1.3829 (16)	C27—H271	1.012 (16)
C13—H13	0.979 (14)	C27—H272	0.962 (15)
C14—C15	1.3841 (16)	C28—H281	1.005 (17)
C14—H14	0.953 (14)	C28—H282	0.991 (16)
C15—C16	1.4934 (16)	C28—H283	0.995 (18)
C16—H161	0.94 (2)	O31—C31	1.2940 (17)
C16—H162	0.97 (2)	O31—H31	1.09 (2)
C16—H163	0.93 (2)	O32—C31	1.2257 (15)
C17—C18	1.520 (2)	O33—C33	1.2417 (15)
C17—H171	0.986 (15)	O34—C33	1.2639 (16)
C17—H172	0.957 (16)	C31—C32	1.5113 (16)
C18—H181	1.02 (2)	C32—C33	1.5215 (17)
C18—H182	0.999 (18)	C32—H321	0.991 (16)
C18—H183	0.966 (19)	C32—H322	0.924 (16)
N2—C21	1.3465 (14)	O41—C41	1.2914 (16)
N2—C25	1.3545 (15)	O41—H41	1.04 (2)
N2—H21	0.927 (17)	O42—C41	1.2288 (14)
O2—C22	1.3388 (14)	O43—C43	1.2406 (15)
O2—H22	0.96 (2)	O44—C43	1.2683 (15)
C21—C22	1.3984 (16)	C41—C42	1.5078 (17)
C21—C27	1.4986 (16)	C42—C43	1.5257 (16)
C22—C23	1.3902 (16)	C42—H421	0.944 (19)
C23—C24	1.3888 (16)	C42—H422	0.985 (18)

C12—O1—H12	108.6 (11)	C25—C24—H24	117.9 (8)
C15—N1—C11	125.23 (10)	C23—C24—H24	121.6 (8)
C15—N1—H11	118.6 (9)	N2—C25—C24	117.49 (10)
C11—N1—H11	116.2 (9)	N2—C25—C26	118.34 (10)
N1—C11—C12	117.75 (10)	C24—C25—C26	124.18 (11)
N1—C11—C17	118.57 (10)	C25—C26—H261	111.0 (10)
C12—C11—C17	123.63 (10)	C25—C26—H262	112.7 (10)
O1—C12—C13	123.55 (10)	H261—C26—H262	105.0 (14)
O1—C12—C11	117.31 (10)	C25—C26—H263	109.7 (11)
C13—C12—C11	119.13 (10)	H261—C26—H263	110.9 (14)
C14—C13—C12	120.07 (11)	H262—C26—H263	107.4 (14)
C14—C13—H13	121.5 (8)	C21—C27—C28	112.70 (10)
C12—C13—H13	118.5 (8)	C21—C27—H271	108.0 (9)
C13—C14—C15	120.33 (11)	C28—C27—H271	108.2 (9)
C13—C14—H14	123.0 (8)	C21—C27—H272	108.1 (9)
C15—C14—H14	116.7 (8)	C28—C27—H272	109.9 (8)
N1—C15—C14	117.45 (10)	H271—C27—H272	109.9 (12)
N1—C15—C16	118.48 (10)	C27—C28—H281	111.0 (9)
C14—C15—C16	124.08 (11)	C27—C28—H282	108.0 (9)

C15—C16—H161	112.3 (12)	H281—C28—H282	109.5 (12)
C15—C16—H162	112.2 (12)	C27—C28—H283	113.1 (10)
H161—C16—H162	104.6 (16)	H281—C28—H283	107.8 (13)
C15—C16—H163	113.1 (12)	H282—C28—H283	107.5 (13)
H161—C16—H163	106.1 (16)	C31—O31—H31	103.1 (12)
H162—C16—H163	107.9 (16)	C33—O34—H31	101.0 (9)
C11—C17—C18	111.01 (11)	O32—C31—O31	123.34 (12)
C11—C17—H171	110.0 (9)	O32—C31—C32	119.43 (12)
C18—C17—H171	109.8 (9)	O31—C31—C32	117.23 (11)
C11—C17—H172	108.5 (9)	C31—C32—C33	117.58 (11)
C18—C17—H172	111.8 (9)	C31—C32—H321	108.4 (9)
H171—C17—H172	105.6 (12)	C33—C32—H321	107.7 (9)
C17—C18—H181	108.5 (11)	C31—C32—H322	107.7 (9)
C17—C18—H182	112.2 (10)	C33—C32—H322	107.5 (9)
H181—C18—H182	110.5 (15)	H321—C32—H322	107.5 (13)
C17—C18—H183	110.4 (11)	O33—C33—O34	124.93 (12)
H181—C18—H183	111.7 (16)	O33—C33—C32	116.76 (12)
H182—C18—H183	103.5 (15)	O34—C33—C32	118.31 (11)
C21—N2—C25	125.04 (10)	C41—O41—H41	103.5 (12)
C21—N2—H21	119.2 (10)	C43—O44—H41	100.7 (9)
C25—N2—H21	115.7 (10)	O42—C41—O41	122.92 (11)
C22—O2—H22	115.1 (12)	O42—C41—C42	120.08 (11)
N2—C21—C22	117.81 (10)	O41—C41—C42	116.99 (10)
N2—C21—C27	119.08 (10)	C41—C42—C43	116.76 (11)
C22—C21—C27	123.11 (10)	C41—C42—H421	110.1 (11)
O2—C22—C23	123.86 (10)	C43—C42—H421	110.2 (11)
O2—C22—C21	116.74 (10)	C41—C42—H422	106.5 (11)
C23—C22—C21	119.39 (10)	C43—C42—H422	105.7 (10)
C24—C23—C22	119.83 (10)	H421—C42—H422	107.0 (15)
C24—C23—H23	121.0 (8)	O43—C43—O44	125.41 (11)
C22—C23—H23	119.2 (8)	O43—C43—C42	117.02 (11)
C25—C24—C23	120.43 (11)	O44—C43—C42	117.57 (11)

C15—N1—C11—C12	1.50 (18)	N2—C21—C22—C23	0.76 (17)
C15—N1—C11—C17	−176.24 (11)	C27—C21—C22—C23	−178.72 (11)
N1—C11—C12—O1	179.24 (10)	O2—C22—C23—C24	−179.54 (11)
C17—C11—C12—O1	−3.13 (18)	C21—C22—C23—C24	−0.47 (18)
N1—C11—C12—C13	0.19 (17)	C22—C23—C24—C25	−0.51 (18)
C17—C11—C12—C13	177.81 (11)	C21—N2—C25—C24	−0.89 (17)
O1—C12—C13—C14	179.87 (11)	C21—N2—C25—C26	179.01 (11)
C11—C12—C13—C14	−1.14 (18)	C23—C24—C25—N2	1.16 (17)
C12—C13—C14—C15	0.53 (18)	C23—C24—C25—C26	−178.74 (12)
C11—N1—C15—C14	−2.11 (18)	N2—C21—C27—C28	108.67 (13)
C11—N1—C15—C16	177.54 (11)	C22—C21—C27—C28	−71.86 (16)
C13—C14—C15—N1	1.02 (18)	O32—C31—C32—C33	178.67 (12)
C13—C14—C15—C16	−178.60 (12)	O31—C31—C32—C33	−1.77 (18)
N1—C11—C17—C18	92.62 (14)	C31—C32—C33—O33	179.68 (11)
C12—C11—C17—C18	−84.99 (16)	C31—C32—C33—O34	−0.52 (18)

C25—N2—C21—C22	−0.07 (17)	O42—C41—C42—C43	−163.63 (12)
C25—N2—C21—C27	179.43 (11)	O41—C41—C42—C43	17.38 (18)
N2—C21—C22—O2	179.89 (10)	C41—C42—C43—O43	163.73 (12)
C27—C21—C22—O2	0.42 (17)	C41—C42—C43—O44	−17.02 (18)

Hydrogen-bond geometry (Å, º)

D—H···*A*	*D*—H	H···*A*	*D*···*A*	*D*—H···*A*
O31—H31···O34	1.09 (2)	1.38 (2)	2.4410 (13)	162 (2)
O41—H41···O44	1.04 (2)	1.44 (2)	2.4428 (12)	162 (2)
O1—H12···O33	0.901 (19)	1.69 (2)	2.5925 (13)	175.0 (17)
O2—H22···O43	0.96 (2)	1.62 (2)	2.5610 (12)	167.6 (19)
N2—H21···O32	0.927 (17)	1.800 (17)	2.7196 (13)	170.9 (15)
N1—H11···O42^{i}	0.918 (15)	1.850 (16)	2.7604 (13)	171.1 (13)

Symmetry code: (i) *x*−1, *y*+2, *z*+1.

2-Ethyl-3-hydroxy-6-methylpyridin-1-ium 6-carboxyhexanoate (III)

Crystal data

$C_8H_{12}NO^+·C_6H_9O_4^-$
M_r = 283.32
Triclinic, $P\overline{1}$
Hall symbol: -P 1
a = 8.7831 (17) Å
b = 8.9442 (17) Å
c = 9.6114 (18) Å
α = 77.301 (3)°
β = 76.142 (3)°
γ = 85.677 (3)°
V = 714.9 (2) Å^3
Z = 2
F(000) = 304
D_x = 1.316 Mg m^{-3}
Mo *Kα* radiation, *λ* = 0.71073 Å
Cell parameters from 2982 reflections
θ = 2.4–30.3°
μ = 0.10 mm^{-1}
T = 150 K
Prism, colourless
0.45 × 0.40 × 0.30 mm

Data collection

Bruker SMART APEXII diffractometer
Radiation source: fine-focus sealed tube
Graphite monochromator
ω scans
Absorption correction: multi-scan (SADABS; Bruker, 2008)
T_{min} = 0.957, T_{max} = 0.971
6841 measured reflections
3122 independent reflections
2569 reflections with $I > 2\sigma(I)$
R_{int} = 0.021
θ_{max} = 27.0°, θ_{min} = 2.2°
h = −11→11
k = −11→11
l = −12→12

Refinement

Refinement on F^2
Least-squares matrix: full
$R[F^2 > 2\sigma(F^2)]$ = 0.041
$wR(F^2)$ = 0.114
S = 1.05
3122 reflections
265 parameters
0 restraints
Primary atom site location: structure-invariant direct methods
Secondary atom site location: difference Fourier map
Hydrogen site location: difference Fourier map
All H-atom parameters refined
$w = 1/[\sigma^2(F_o^2) + (0.0678P)^2 + 0.0968P]$ where $P = (F_o^2 + 2F_c^2)/3$
$(\Delta/\sigma)_{max} < 0.001$
$\Delta\rho_{max}$ = 0.26 e Å^{-3}
$\Delta\rho_{min}$ = −0.22 e Å^{-3}

Special details

Geometry. All esds (except the esd in the dihedral angle between two l.s. planes) are estimated using the full covariance matrix. The cell esds are taken into account individually in the estimation of esds in distances, angles and torsion angles; correlations between esds in cell parameters are only used when they are defined by crystal symmetry. An approximate (isotropic) treatment of cell esds is used for estimating esds involving l.s. planes.

Refinement. Refinement of F^2 against ALL reflections. The weighted R-factor wR and goodness of fit S are based on F^2, conventional R-factors R are based on F, with F set to zero for negative F^2. The threshold expression of $F^2 > 2\text{sigma}(F^2)$ is used only for calculating R-factors(gt) etc. and is not relevant to the choice of reflections for refinement. R-factors based on F^2 are statistically about twice as large as those based on F, and R- factors based on ALL data will be even larger.

Fractional atomic coordinates and isotropic or equivalent isotropic displacement parameters (Å²)

	x	*y*	*z*	U_{iso}*/U_{eq}
O1	−0.20593 (11)	0.62338 (11)	0.11713 (10)	0.0292 (2)
H2	−0.228 (2)	0.700 (2)	0.047 (2)	0.064 (6)*
N1	0.13170 (12)	0.45634 (12)	0.23947 (11)	0.0211 (2)
H1	0.153 (2)	0.375 (2)	0.306 (2)	0.041 (5)*
C1	−0.01767 (14)	0.47705 (14)	0.22500 (13)	0.0208 (3)
C2	−0.05585 (15)	0.60828 (14)	0.12762 (13)	0.0221 (3)
C3	0.06186 (16)	0.71071 (15)	0.05091 (14)	0.0245 (3)
C4	0.21377 (16)	0.68091 (15)	0.06912 (14)	0.0249 (3)
C5	0.25044 (14)	0.55150 (14)	0.16525 (13)	0.0227 (3)
C6	0.41058 (16)	0.50777 (18)	0.19083 (16)	0.0296 (3)
C7	−0.13652 (15)	0.36075 (14)	0.31264 (14)	0.0243 (3)
C8	−0.24304 (19)	0.41427 (18)	0.44312 (17)	0.0348 (3)
H3	0.0377 (18)	0.8016 (19)	−0.0186 (18)	0.034 (4)*
H4	0.2981 (18)	0.7486 (18)	0.0168 (17)	0.027 (4)*
H61	0.410 (3)	0.493 (2)	0.285 (3)	0.067 (6)*
H62	0.447 (2)	0.420 (2)	0.154 (2)	0.047 (5)*
H63	0.487 (2)	0.585 (2)	0.143 (2)	0.049 (5)*
H71	−0.0840 (18)	0.2653 (18)	0.3421 (17)	0.031 (4)*
H72	−0.1990 (19)	0.3413 (18)	0.2460 (19)	0.036 (4)*
H81	−0.180 (2)	0.430 (2)	0.510 (2)	0.053 (5)*
H82	−0.296 (2)	0.512 (2)	0.413 (2)	0.052 (5)*
H83	−0.321 (2)	0.339 (2)	0.4962 (19)	0.040 (4)*
O11	−0.00039 (12)	0.15146 (13)	0.59754 (12)	0.0434 (3)
H11	−0.051 (3)	0.068 (3)	0.692 (3)	0.088 (8)*
O12	0.22294 (11)	0.23943 (11)	0.45206 (10)	0.0300 (2)
O13	0.89348 (11)	−0.04695 (12)	0.81496 (12)	0.0393 (3)
O14	0.68104 (11)	−0.17891 (11)	0.93355 (10)	0.0315 (2)
C11	0.15037 (15)	0.15899 (14)	0.56614 (14)	0.0248 (3)
C12	0.23604 (15)	0.06199 (16)	0.67565 (16)	0.0278 (3)
C13	0.40362 (14)	0.10703 (14)	0.65759 (14)	0.0223 (3)
C14	0.48701 (14)	−0.00703 (14)	0.76002 (14)	0.0232 (3)
C15	0.65418 (15)	0.03752 (15)	0.74244 (15)	0.0244 (3)
C16	0.74819 (14)	−0.07165 (14)	0.83756 (14)	0.0237 (3)
H121	0.239 (2)	−0.044 (2)	0.658 (2)	0.047 (5)*
H122	0.175 (2)	0.0607 (19)	0.770 (2)	0.039 (4)*

H131	0.4583 (18)	0.1133 (17)	0.5562 (18)	0.028 (4)*
H132	0.4040 (18)	0.2086 (18)	0.6765 (17)	0.031 (4)*
H141	0.4301 (19)	−0.0117 (18)	0.8594 (19)	0.034 (4)*
H142	0.4890 (16)	−0.1073 (17)	0.7352 (16)	0.023 (4)*
H151	0.7129 (18)	0.0471 (18)	0.6417 (19)	0.032 (4)*
H152	0.6544 (19)	0.138 (2)	0.7678 (19)	0.039 (4)*

Atomic displacement parameters (Å²)

	U^{11}	U^{22}	U^{33}	U^{12}	U^{13}	U^{23}
O1	0.0238 (5)	0.0301 (5)	0.0287 (5)	0.0001 (4)	−0.0120 (4)	0.0106 (4)
N1	0.0235 (6)	0.0200 (5)	0.0181 (5)	−0.0001 (4)	−0.0079 (4)	0.0032 (4)
C1	0.0231 (6)	0.0208 (6)	0.0174 (6)	0.0003 (5)	−0.0070 (5)	0.0003 (5)
C2	0.0239 (6)	0.0228 (6)	0.0184 (6)	0.0021 (5)	−0.0078 (5)	0.0005 (5)
C3	0.0303 (7)	0.0217 (6)	0.0186 (6)	−0.0003 (5)	−0.0075 (5)	0.0040 (5)
C4	0.0272 (7)	0.0245 (6)	0.0201 (6)	−0.0049 (5)	−0.0050 (5)	0.0023 (5)
C5	0.0235 (6)	0.0250 (6)	0.0185 (6)	−0.0015 (5)	−0.0055 (5)	−0.0011 (5)
C6	0.0230 (7)	0.0375 (8)	0.0244 (7)	−0.0015 (6)	−0.0056 (5)	0.0022 (6)
C7	0.0253 (6)	0.0210 (6)	0.0248 (6)	−0.0021 (5)	−0.0100 (5)	0.0040 (5)
C8	0.0350 (8)	0.0315 (8)	0.0292 (7)	−0.0033 (6)	−0.0004 (6)	0.0050 (6)
O11	0.0224 (5)	0.0530 (7)	0.0418 (6)	−0.0050 (5)	−0.0145 (4)	0.0269 (5)
O12	0.0259 (5)	0.0304 (5)	0.0279 (5)	−0.0019 (4)	−0.0110 (4)	0.0119 (4)
O13	0.0226 (5)	0.0459 (6)	0.0404 (6)	−0.0045 (4)	−0.0153 (4)	0.0205 (5)
O14	0.0254 (5)	0.0316 (5)	0.0313 (5)	−0.0018 (4)	−0.0124 (4)	0.0134 (4)
C11	0.0220 (6)	0.0229 (6)	0.0273 (7)	−0.0020 (5)	−0.0113 (5)	0.0064 (5)
C12	0.0216 (7)	0.0282 (7)	0.0285 (7)	−0.0028 (5)	−0.0111 (6)	0.0118 (6)
C13	0.0204 (6)	0.0203 (6)	0.0238 (7)	−0.0004 (5)	−0.0088 (5)	0.0049 (5)
C14	0.0197 (6)	0.0229 (6)	0.0234 (7)	−0.0004 (5)	−0.0079 (5)	0.0059 (5)
C15	0.0214 (6)	0.0229 (6)	0.0260 (7)	−0.0007 (5)	−0.0103 (5)	0.0059 (5)
C16	0.0219 (6)	0.0241 (6)	0.0228 (6)	0.0005 (5)	−0.0087 (5)	0.0033 (5)

Geometric parameters (Å, º)

O1—C2	1.3405 (15)	C8—H82	0.97 (2)
O1—H2	0.90 (2)	C8—H83	0.970 (18)
N1—C1	1.3470 (16)	O11—C11	1.2892 (16)
N1—C5	1.3533 (16)	O11—H11	1.07 (3)
N1—H1	0.90 (2)	O12—C11	1.2303 (15)
C1—C2	1.4050 (16)	O13—C16	1.2701 (16)
C1—C7	1.4962 (17)	O14—C16	1.2470 (16)
C2—C3	1.3901 (18)	C11—C12	1.5187 (16)
C3—C4	1.3856 (19)	C12—C13	1.5149 (18)
C3—H3	0.977 (17)	C12—H121	0.994 (19)
C4—C5	1.3832 (17)	C12—H122	0.933 (18)
C4—H4	0.961 (16)	C13—C14	1.5290 (16)
C5—C6	1.4940 (18)	C13—H131	0.970 (16)
C6—H61	0.89 (2)	C13—H132	0.965 (16)
C6—H62	0.931 (19)	C14—C15	1.5109 (18)

C6—H63	0.96 (2)	C14—H141	0.959 (17)
C7—C8	1.520 (2)	C14—H142	0.975 (15)
C7—H71	0.958 (16)	C15—C16	1.5227 (16)
C7—H72	0.986 (17)	C15—H151	0.971 (16)
C8—H81	0.98 (2)	C15—H152	0.984 (17)
C2—O1—H2	115.9 (13)	C7—C8—H83	110.9 (10)
C1—N1—C5	125.04 (11)	H81—C8—H83	108.5 (15)
C1—N1—H1	117.5 (11)	H82—C8—H83	109.0 (15)
C5—N1—H1	117.4 (11)	C11—O11—H11	115.9 (13)
N1—C1—C2	118.33 (11)	O12—C11—O11	122.00 (11)
N1—C1—C7	119.23 (10)	O12—C11—C12	120.95 (11)
C2—C1—C7	122.44 (11)	O11—C11—C12	117.04 (11)
O1—C2—C3	125.40 (11)	C13—C12—C11	114.88 (11)
O1—C2—C1	115.97 (11)	C13—C12—H121	107.7 (10)
C3—C2—C1	118.63 (11)	C11—C12—H121	105.2 (11)
C4—C3—C2	120.02 (11)	C13—C12—H122	112.8 (10)
C4—C3—H3	120.3 (9)	C11—C12—H122	108.3 (11)
C2—C3—H3	119.6 (9)	H121—C12—H122	107.4 (15)
C5—C4—C3	121.00 (12)	C12—C13—C14	111.48 (10)
C5—C4—H4	116.9 (9)	C12—C13—H131	108.6 (9)
C3—C4—H4	122.1 (9)	C14—C13—H131	110.8 (9)
N1—C5—C4	116.95 (11)	C12—C13—H132	109.4 (9)
N1—C5—C6	117.92 (11)	C14—C13—H132	110.1 (9)
C4—C5—C6	125.12 (12)	H131—C13—H132	106.4 (13)
C5—C6—H61	110.7 (14)	C15—C14—C13	111.65 (10)
C5—C6—H62	109.7 (11)	C15—C14—H141	109.8 (10)
H61—C6—H62	111.1 (18)	C13—C14—H141	109.1 (10)
C5—C6—H63	113.4 (11)	C15—C14—H142	108.3 (8)
H61—C6—H63	105.5 (17)	C13—C14—H142	108.1 (9)
H62—C6—H63	106.3 (15)	H141—C14—H142	109.9 (13)
C1—C7—C8	112.50 (11)	C14—C15—C16	115.48 (10)
C1—C7—H71	109.4 (9)	C14—C15—H151	111.2 (9)
C8—C7—H71	111.7 (9)	C16—C15—H151	106.9 (9)
C1—C7—H72	107.1 (10)	C14—C15—H152	109.4 (10)
C8—C7—H72	110.2 (9)	C16—C15—H152	106.4 (10)
H71—C7—H72	105.6 (13)	H151—C15—H152	107.1 (14)
C7—C8—H81	109.1 (11)	O14—C16—O13	123.05 (11)
C7—C8—H82	111.7 (11)	O14—C16—C15	119.66 (11)
H81—C8—H82	107.5 (15)	O13—C16—C15	117.29 (11)
C5—N1—C1—C2	−1.12 (18)	C3—C4—C5—N1	0.17 (19)
C5—N1—C1—C7	179.02 (11)	C3—C4—C5—C6	178.91 (13)
N1—C1—C2—O1	179.93 (10)	N1—C1—C7—C8	103.03 (14)
C7—C1—C2—O1	−0.21 (18)	C2—C1—C7—C8	−76.83 (16)
N1—C1—C2—C3	−0.09 (18)	O12—C11—C12—C13	17.5 (2)
C7—C1—C2—C3	179.77 (12)	O11—C11—C12—C13	−163.33 (13)
O1—C2—C3—C4	−178.77 (12)	C11—C12—C13—C14	−173.44 (12)

C1—C2—C3—C4	1.25 (19)	C12—C13—C14—C15	−179.96 (12)
C2—C3—C4—C5	−1.3 (2)	C13—C14—C15—C16	−178.57 (12)
C1—N1—C5—C4	1.07 (18)	C14—C15—C16—O14	−7.79 (19)
C1—N1—C5—C6	−177.76 (12)	C14—C15—C16—O13	172.81 (12)

Hydrogen-bond geometry (Å, º)

D—H···*A*	*D*—H	H···*A*	*D*···*A*	*D*—H···*A*
O11—H11···O13^{i}	1.07 (3)	1.40 (3)	2.4639 (15)	176 (2)
O1—H2···O14^{ii}	0.90 (2)	1.66 (2)	2.5355 (12)	163 (2)
N1—H1···O12	0.90 (2)	1.83 (2)	2.7181 (14)	167.6 (16)

Symmetry codes: (i) $x-1, y, z$; (ii) $x-1, y+1, z-1$.